Comet 9P/Tempel 1: sublimation beneath the dust cover

Konrad J. Kossacki, Slawomira Szutowicz

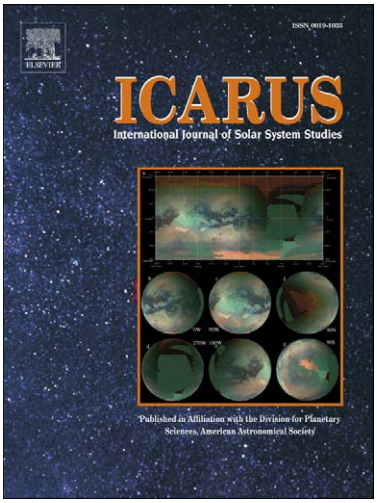

Comet 9P/Tempel 1: sublimation beneath the dust cover

Konrad J. Kossacki, Slawomira Szutowicz

PII: S0019-1035(08)00024-9
DOI: 10.1016/j.icarus.2007.12.014
Reference: YICAR 8569

To appear in: *Icarus*

Received date: 9 July 2007
Revised date: 10 July 2007
Accepted date: 13 December 2007

Please cite this article as: K.J. Kossacki, S. Szutowicz, Comet 9P/Tempel 1: sublimation beneath the dust cover, *Icarus* (2008), doi: 10.1016/j.icarus.2007.12.014

Comet 9P/Tempel 1: sublimation beneath the dust cover

Konrad J. Kossacki

Institute of Geophysics of Warsaw University, Pasteura 7,02-093 Warsaw, Poland

E-mail: kjkossac@igf.fuw.edu.pl

Slawomira Szutowicz

Space Research Center of Polish Academy of Sciences, Bartycka 18a, 00-716, Warsaw, Poland

Number of pages (including figures): 56

Number of tables: 2

Number of figures: 13

Preprint submitted to Elsevier Science *16 January 2008*

Please send Editorial Correspondence to:

Konrad J. Kossacki

Institute of Geophysics of Warsaw University

Pasteura 7

02-093 Warsaw, POLAND

Tel: (48) 22 5546834

Fax: (48) 22 5546882

E-mail: kjkossac@igf.fuw.edu.pl

Proposed Running Head:

Sub-dust sublimation

Abstract

In the current work we analyze properties of the dust mantle, its thickness and thermal conductivity, necessary to reproduce observed rate of water production of comet 9P/Tempel 1. For this purpose we considered simplified shape of the comet nucleus approximated by the symmetric prolate ellipsoid with smooth surface. We have performed simulations, using models with dust mantle of the thickness either constant, but nonuniform (Model A), or evolving (Model B). The simulated profiles of water production versus time were compared with observations. In addition, we compared the calculated surface temperature with the real temperatures derived from IR observations (the Deep Impact mission). This new double-stage verification procedure, shows that our model A is a good representation for the nucleus of comet Tempel 1. This indicates, that the dust mantle thickness should be nonuniform, but does not change significantly with time. We show, that reproducing observed high temperatures of the nucleus requires dust mantle, that is almost everywhere thick and has extremely low thermal inertia. The latter should be close to zero as already predicted by others. The agreement between the simulated and measured water production can be obtained when the dust is regionally thin and has the thermal inertia higher than average, according to our simulations about 100 $\mathrm{W\,s^{1/2}\,K^{-1}\,m^{-2}}$. Such regions should be located in the south hemisphere of the nucleus.

Key words: Comets, composition, Ices

1 Introduction

The small-distance observations during Deep Impact mission in 2005 provided high resolution images of Comet Tempel 1. They revealed 'evidence of extensive surface erosion', 'crater-like depressions' and 'occurrence of very smooth terrains' (A'Hearn et al., 2005). According to Sunshine et al. (2006) ice is present only on the area 0.49 - 0.55 km^2 of the observed part of the nucleus, that is on about 0.5% of the total surface. Moreover, the detected ice is only admixture in dust. As a result, the surface area of only $\sim$0.03 km^2 contains a pure water ice. It cannot be excluded, that on the other side of the nucleus is more exposed ice. However, this seems not very likely. Sunshine et al. (2006) concludes, that if the distribution of ice is roughly the same on the whole nucleus the observed outgassing of comet Tempel 1 has extensive subsurface sources. Davidsson et al. (2007) have found based on their thermophysical simulations that the area of $\sim$ 3.1 km^2 of the surface should be covered by the exposed ice to reproduce the observed sublimation rate, two orders of magnitude more than the ice coverage estimated by Sunshine et al. (2006) for the imaged side of the nucleus. This discrepancy indicates dominating role of the sub-dust outgassing of the nucleus, the process simulated in the current paper. Activity of known cometary nuclei is concentrated in some regions. Typically, regions of high activity are considered as free, or almost free of dust. We propose the model of the active regions on comet 9P/Tempel 1 as covered by a thin dust mantle.

In the present work we investigate how properties of the dust mantle, and their possible evolution affect water production from the considered comet. We attempt to determine thermal inertia of the dust mantle and spatial dis-

tribution of the dust thickness. For this purpose we compare the results of simulations with the observed water production from the nucleus versus time and with the temperature map of the nucleus. The former are reconstructed from various types of observations, including brightness of the comet, while the latter was determined from the IR spacecraft observations (A'Hearn et al., 2005; Groussin et al., 2007). We focus attention on the properties of the dust mantle, not on the precise reproduction of the observed, topography dependent temperature distribution. Thus, we consider smooth nucleus modeled as a prolate ellipsoid. The surface of the nucleus is covered by a dust layer and the activity is driven by sublimation of the subsurface ice. Our model describing evolution of the dust covered nucleus was originally developed to study properties of comet 46P/Wirtanen (Kossacki et al., 1999). Newer version was successfully tested using observations of comet 67P/Churyumov-Gerasimenko (Kossacki and Szutowicz, 2006). For the purpose of the current research we have extended our model. The most important is including dynamical changes of the dust mantle. Thickness of the modeled dust cover can either remain constant, or undergo changes. In the latter case, the dust mantle increases in thickness due to sublimation of ice beneath the dust and episodically is blown-out.

2 Description of the model

2.1 Basic properties

In our work we use model of the comet nucleus based on this presented in Kossacki et al. (2006); Kossacki and Szutowicz (2006). The model calculates

the temperature and cohesity distribution versus depth, and the water emission to space. The new features are: the non-spherical shape of the nucleus, and the evolving thickness of the dust mantle. Below we summarize the basic properties of the model.

The nucleus matter is assumed to be composed of mineral/icy grains with minerals in their centers and ice forming their surfaces. The surface of the nucleus is covered by the dust mantle. Local thickness of the dust layer is either constant, or evolves. Ice sublimes beneath the dust layer and the vapor migrates partially through the dust to space and partially downward to the interior of the nucleus. The latter is followed by the condensation of vapor and hence leads to the decrease of porosity beneath the ice-dust interface. The surface temperature of the dust layer is determined by the variable illumination, and the heat transport through the dust. The latter depends on the dust properties, i.e. the thermal conductivity, the density and the specific heat, as well as on the dust thickness and the temperature beneath the dust. At the interface between the dust mantle and the deeper part of the nucleus the temperature is calculated from the energy balance including heat transport below and above the interface, as well as the energy losses due to sublimation of ice at the interface. The flux of light absorbed at the dust surface depends on the local orientation of the surface, that is function of the latitude and the nucleus oblateness, and on the current position of the Sun relative to the comet. The latter evolves due to the orbital motion and rotation of the comet. The changes of illumination in the diurnal and orbital cycles affect the distribution of temperature on the surface, hence also sublimation rate of ice below the dust mantle. In addition, roughness of the surface, may enhance non-uniformity of the surface temperature and hence non-uniformity of the ice sublimation. For

example, local self-heating of the surface due to multiple scattering of radiation in craters, or depressions may noticeably enhance sublimation at low zenithal angle of the Sun. However, in the current work we focus attention on the properties dust mantle itself, not on the precise reproduction of the topography dependent temperature map of the nucleus. Thus, for our purpose it is sufficient to assume smooth cometary surface. The diffusion of heat in the comet nucleus depends on the local structure of the material and on the temperature. In our model structure of the material beneath the dust mantle evolves, due to sintering of ice mantled grains. The dust layer has constant properties, except thickness.

In the Section 2.2 we describe our model. Sections 2.2.1 and 2.2.2 are to present basic equations specific for the dust mantle and for the underlying matrix of ice-dust grains, respectively. In the Section 2.2.3 we present boundary conditions.

2.2 Mathematical formulation

The rate of ice sublimation beneath the dust mantle depends on the local heat balance, hence on the illumination, as well as on the thermal conductivity of the dust layer and of the underlying material. The thermal properties of the dust mantle are independent on the temperature. However, the underlying matrix of ice-dust grains strongly reacts on the temperature. This is due to the temperature dependent thermal conductivity of ice, but also due to the temperature driven sintering of the grains. Thus, in addition to the formula describing sublimation of water ice beneath the dust mantle we have to solve equations for changes of the temperature, the Hertz factor and the porosity.

The model has five parameters describing structure of the material composing comet nucleus beneath the dust cover and three parameters describing structure of the dust mantle. For the ice-dust material underlying the dust we have: radius of the grains r_g, effective radius of the pores r_p, tortuosity of the pores τ, porosity ψ and the Hertz factor h. The radii r_g and r_p can change only very little, as we discuss in the Section 3.2. Thus, in the current work we keep $r_g = r_p$, that reduces the number of parameters for the parameters to four. The parameters ψ, and h are variable, they evolve due to condensation of the vapor migrating downward from the bottom of the dust mantle. The porosity can be expressed in terms of the dimensionless volume of ice v_i and volume of minerals v_s in the comet nucleus, $\psi = 1 - v_i - v_s$. The Hertz factor is defined as the ratio between the grain-to-grain contact area and the cross-section of a grain. Then $h = (r_n/r_g)^2$, where r_n is the radius of the grain-to grain contact area. The sintering process considered in our work, so called Kelvin effect, modifies the cohesivity of the cometary material, but does not influence its porosity. High cohesivity concerns the medium with the Hertz factor about 0.1 and low cohesivity concerns the medium with h much lower. We describe the structure of the dust layer by the effective pore radius r_d, tortuosity of the pores τ and the porosity ψ_d. In most cases we assume that $r_d = 2r_p$ (Section 3.1). The thermal conductivity of the dust layer λ_d is constant. The dust thickness Δ_d is constant in one of the sub-models called A, and evolves in the other one called B.

2.2.1 Dust mantle

The thickness of the dust layer, as well as its thermal conductivity, may evolve with time. Some processes tend to increase its thickness, while some others

reduce it. Evolution of the dust mantle was considered by several authors, e.g. Brin and Mendis (1979), Kührt and Keller (1994), Orosei et al. (1995), Rickman et al. (1990). Sublimation of ice from beneath the dust cover results in the growth of its thickness due to the recession of its bottom (sublimation front of water ice) toward the center of a comet nucleus. The process reducing thickness of the dust layer can be the local blown out of the whole mantle. This should be expected when the gas pressure at the ice-dust interface rises sufficiently. Thus, blow out of dust may be common event. Indeed, outbursts are frequently observed. In contrast, impacts have external origin and are highly unpredictable. The most common small impact events should result only in the gradual erosion of the dust mantle. Some erosion may result also from the transport of small grains by the water vapor through the dust mantle to space. It can also be expected, that some dust particles transported through the dust layer are deposited in small pores. This effect slowly reduces permeability of the layer and hence leads to an increase of gas pressure beneath the dust. However, simulating the evolution of the dust mantle is very time consuming and requires several assumptions about the properties of dust. In our work we attempt to simulate long-term changes of the dust thickness. We focus our attention on the thickening of the dust mantle due to local sublimation of ice beneath the dust and the events of dust blow out.

We consider two different models for the dust mantle. In the basic one, thereafter called Model A, the erosion of the dust layer is compensated by thickening of the dust layer due to the sublimation of ice beneath the dust, i.e. the model assumes constant thickness of the dust layer. This model of the dust mantle we used in Kossacki and Szutowicz (2006).

In the second model, called Model B, dust layer does not experience continu-

ous erosion, but episodically can be blown out. As long as the vapor pressure beneath it is low the thickness of the dust layer continuously increases due to sublimation of ice beneath the dust. When the gas pressure exceeds critical value, being in our model free parameter, the dust is locally blown out. Rickman et al. (1990) considered the dust mantle without cohesion. Thus, they assumed that the blow-off of the dust layer occurs when the gas pressure at the interface between the dust mantle and the underlying ice overcomes the weight of the dust mantle. There exists several works dealing with the possible cohesivity of the dust layer. Kührt and Keller (1994) considered cohesive mantle, that is strongly bounded to the nucleus and never can be blown out. In this case, activity of the comet significantly decreases from apparition to apparition. In our model we do not separate gravitational and cohesive bonding of the dust mantle. The critical vapor pressure p_{max}, corresponding to the blow out of the dust mantle is the free parameter. The overall strength of the excavated material resulting from the Deep Impact experiment was estimated to be < 65 Pa (A'Hearn et al., 2005). Thus, we tested values of p_{max} equal, or lower than 65 Pa. The considered values are lower than the expected strength of the dry dust, that is $10^2 - 10^4$ (Kührt and Keller, 1994). We discuss this problem in greater details in the Section 3.1.

In both models porosity of the dust mantle and its thermal conductivity remain constant. The heat transport equation is

$$\varrho_d c_d \frac{\partial T}{\partial t} = \frac{\partial}{\partial z}\left(\lambda_d \frac{\partial T}{\partial z}\right), \tag{1}$$

where T is temperature, t is time and z is depth below the surface. The other symbols denote material parameters: effective thermal conductivity of the dust λ_d, density of the dust layer ϱ_d, and specific heat of dust c_d.

When the dust is at least 0.5cm thick, that is always the case for Model A and most of the time for Model B, vapor flux is calculated using long tube formula for the diffusion coefficient

$$F_s = \left(\frac{32\mu}{9R\pi T_{int}}\right)^{1/2} \frac{r_d \psi_d}{\tau^2} \frac{p_{sat}(T_{int})}{\Delta_d} \ . \tag{2}$$

For the coefficient under square root different values were used in literature. We follow Kömle and Steiner (1992). The variable T_{int} is the current temperature at the bottom of the dust mantle, p_{sat} is the pressure of the phase equilibrium between ice and vapor, μ is the molar mass of vapor, R is the universal gas constant, r_d is the effective pore radius, ψ_d is the porosity of the dust layer and Δ_d is its thickness (see Section 3.1).

When the dust mantle is thin, diffusion of vapor through the dust layer is calculated using modified Clausing formula

$$F_s = \frac{20 + 8\frac{\Delta_d}{r_d}}{20.0 + 19.0\frac{\Delta_d}{r_d} + 3.0\frac{{\Delta_d}^2}{{r_d}^2}} \left(\frac{32\mu}{9R\pi T_{int}}\right)^{1/2} \frac{\psi_d}{\tau^2} p_{sat}(T_{int}) \ . \tag{3}$$

When compare to the original version of the Clausing formula coefficient under square root is changed from 1/2 to 32/9. We have changed this coefficient to obtain the same asymptotic behavior of Eq. 2 and Eq. 3 at high Δ_d/r_d. We use Eq. 3 when the dust mantle is thinner than the size of our numerical grid cell, that is 0.5 cm for the simulations with Model B. This threshold value is 10 times larger than the largest consider pore radius in the dust mantle $r_d = 0.5$ mm.

2.2.2 Icy medium

In the material composed of the ice-dust grains heat can be transported in different ways. At low temperatures dominates heat transport within the solid matrix of grains, while at the temperature about 200 K heat transport in the pores becomes dominating. In our model we use the effective thermal conductivity λ of the ice-dust medium, including both heat transport through the solid grains and via the pores. The heat transport equation is analogous to Eq. 1. The variables λ_d, ϱ_d, c_d are replaced by: λ, ϱ, and c, respectively. The variable λ depends on the porosity ψ of the medium, on temperature, on thermal conductivity λ_g of the grains, on the heat transfer by vapor, and on the Hertz factor h. In our work

$$\lambda = \lambda_g h (1-\psi)^{2/3} + r_p \psi \Big(\frac{32\mu}{9\pi RT} \Big)^{1/2} H \frac{dp_{sat}}{dT}, \tag{4}$$

(Kossacki et al., 1999; Kossacki and Szutowicz, 2006). The second term in the right hand side was originally applied by Kömle and Steiner (1992). It describes heat transport in the pores. The symbol H denotes the latent heat of sublimation. The porosity decreases due to condensation of vapor migrating downward from the sublimation front beneath the dust mantle. The vapor condenses at highest rate just beneath the sublimation front. However the porosity does not decrease significantly, because the ice-dust interface recedes toward the nucleus center. The Eq. 4 assumes implicitly, that the gas pressure in the pores equals the saturation vapor pressure. Indeed, the deviations from the equilibrium are balanced by the sublimation and condensation processes on a time scale several orders of magnitude shorter than the rotation period of the comet nucleus.

In our model the grains are composed of a mineral core and of an ice mantle. In this case the thermal conductivity of the grains (Haruyama et al., 1993) is

$$\lambda_g = \lambda_i \left[1 + \frac{3v(\lambda_m - \lambda_i)}{2\lambda_i + \lambda_m - v(\lambda_m - \lambda_i)} \right]. \quad (5)$$

The symbols λ_m and λ_i denote thermal conductivity of the mineral core and of the icy mantle, respectively, and v is the ratio of the volume of the minerals contained in the grain to the total volume of the grain.

The Hertz factor evolves due to sintering of ice-dust grains. For the granular water ice at temperatures typical for the illuminated cometary surface, i.e. about 200 K, only one mechanism is important. It is the so-called Kelvin effect. This effect is related to the migration of vapor along the surface of the grains towards their contacts due to the local differences of the phase equilibrium pressure (e.g. Eluszkiewicz *et al.* (1998); Kossacki et al. (1999))

2.2.3 Initial and boundary conditions

In the present work we assume, that initially: (i) The cometary material has uniform temperature, and (ii) The Hertz factor is uniform. The key boundary conditions are those at the surface, and at the interface between the dust layer and the deeper part of the nucleus.

When the flat surface is covered by the dust layer of the thickness larger than the size of the grid cell, the surface temperature of the dust is given by the formula

$$\frac{S_c}{R_h^2}(1 - A)\, max(\cos\alpha, 0) - \sigma\epsilon_d {T_s}^4 - \lambda_d \frac{T_s - T_{int}}{\Delta_d} = 0, \quad (6)$$

where the third term, i.e. the heat flux conducted through the dust, is

$$\lambda_d \frac{T_s - T_{int}}{\Delta_d} = -\lambda \nabla T + H\, F_s. \tag{7}$$

The term ∇T is the temperature gradient in ice at the dust/ice interface, and T_{int} is the temperature at that interface. The parameter A denotes the surface albedo, $S_c = 1360\,\mathrm{W\,m^{-2}}$ is the solar constant, σ is the Stefan-Boltzman constant, ϵ_d is the emissivity of the dust, and R_h is the actual heliocentric distance in AU and α is the zenith angle of the Sun i.e. the angular position of the Sun in relation to the local normal at a given point on the surface.

At the interface between the dust mantle and the underlying medium composed of ice-dust grains the temperature is determined by the energy balance including: heat flux conducted by the dust mantle, heat flux conducted in the underlying ice-dust medium, and the energy losses due to sublimation followed by the water escape to space. These fluxes combine to

$$F_{int} = \lambda_d \frac{T_s - T_{int}}{\Delta_d} + \lambda \nabla T - H\, F_s, \tag{8}$$

where F_s is given by Eq. 2.

When the dust layer has thickness temporarily smaller than the numerical grid cell, we do not consider temperature gradient in dust. Hence, the temperature of the subliming ice beneath thin dust satisfies the equation

$$\frac{S_c}{R_h^2}(1 - A)\, max(\cos\alpha, 0) - \sigma \epsilon {T_s}^4 + \lambda \nabla T - H\, F_s = 0. \tag{9}$$

where the vapor flux of the subliming ice F_s is given by Eq. 3.

2.2.4 Numerical procedure

In our work the nucleus is covered by the dust mantle of nonuniform thickness, from zero to several centimeters. Thus, the depth to the interface between the dust mantle and the deeper part of the nucleus can be either larger, or smaller than the diurnal thermal skin depth. Thus, we need high vertical resolution. The horizontal heat transport is not calculated, because the horizontal scale is much larger than the thermal skin depth in the seasonal time scale. This means, that we need to solve equations only in one dimension, for several locations on the comet nucleus. For each location we perform simulations using equally spaced grid of the cell size 1 cm, or 0.5cm. The latter is used for the simulations dealing with evolving dust mantle. The grid size is initially the same, 20 m for all locations. When the surface recedes due to sub-dust sublimation of ice, the number of the grid points is reduced. When the local position of the surface changes by the distance equal to the grid cell, the uppermost grid point is removed. The depth from the current surface to the bottom of the grid can not become smaller than about 10 m. The recession rate of the surface significantly depends on the parameters describing dust mantle. At the latitude being subsolar at perihelion the highest recession rate of the surface is about 2 meters per orbit. The time step of calculations depends on the heliocentric distance. For the simulations with the dust mantle of constant thickness the time step is $P_{rot}/300$ when the distance to the Sun R_h is smaller than 2 AU, and $P_{rot}/150$ for larger R_h. When the dust mantle can be blown-out the time steps are: $P_{rot}/1700$ for $R_h < 2$ AU, $P_{rot}/900$ for $2\text{AU} < R_h < 3\text{AU}$ and $P_{rot}/300$ for larger R_h. The integration algorithm is implicit, of the second order accuracy.

Surface of the nucleus is divided into a set of sectors (facets) of equal areas,

evolving independently of each other. The surface temperatures, dust thicknesses and rates of vapor emission are the same for all location in any given sector. Properties of the subsurface layer of the nucleus below a given sector are only functions of depth. Thus, equations are solved only for the middle of each sector. For these points we calculate directions locally normal to the surface. They are used to calculate current local positions of the Sun relative to the surface and hence to find current surface temperature and the emission of water vapor. The minimum number of the needed facets is found to be 32 per the whole nucleus. We have checked that in most cases the resulted water production profiles do not differ from the profiles produced with a larger number of sectors i.e. using 128 sectors. Thus, to save computation time we decided to consider the nucleus divided into only 32 sectors called also thereafter facets. Each facet covers about 0.03 of the total surface of the nucleus. This would be insufficient to account for the influence of the nucleus topography. However, in the current paper we are interested in the general properties of the dust mantle, not in the local differences related to the nucleus topography.

The nucleus is modeled as a prolate ellipsoid rotating around one of the short axes. In Fig. 1 we shown sketch of four sectors of equal surface. For clarity we have drawn only one quarter of the north hemisphere. Centers of the sectors have latitudes l_i and longitudes g_i, where i denotes sector number. For simplicity of geometrical calculations zero longitude corresponds to the equatorial bulge of the considered idealized nucleus. Thus, all our longitudes are shifted by about 40^o relative to the grid defined in Thomas et al. (2007). Centers of our sectors are located as presented in the Table 1.

The Fig. 2 is to demonstrate role of the resolution: vertical, and horizontal. The former is represented by the size of grid cell and the latter is expressed by

the number of sectors on surface of our model nucleus. In the figure are shown theoretical water production curves versus time from perihelion, calculated assuming different resolutions of the depth grid, dz, (lower panel) and different numbers of facets on the model nucleus (upper panel). The nucleus is composed of the grains with the radii $r_g = 0.05$mm. Thickness of the dust mantle is constant versus time (Model A). Dust layer has thermal conductivity $\lambda_d = 20\ \mathrm{mW\,m^{-1}\,K^{-1}}$, uniform thickness 1 cm, and the pore radii either 0.1mm, or 0.05mm. It can be seen, that it is sufficient to perform simulations with 1 cm vertical resolution. The number of sectors on the nucleus surface also does not need to be very large, it is sufficient to consider 32 sectors.

3 Parameters

The current work is focused on the problem, how evolution of the dust mantle affects water production from the comet. Thus, the most important parameters are those characterizing the dust mantle: the porosity ψ_d, the thermal conductivity λ_d and the thickness of dust layer Δ_d. The parameter ψ_d has to be estimated. The thickness Δ_d is in our work either free parameter (Model A), or variable (Model B). In the following two subsections we describe material parameters used in our model. The values of the model parameters used in Model A and Model B are summarized in Table 2.

3.1 Dust Mantle

In the basic Model A the dust mantle has thickness constant with time, uniform, or non-uniform. In the Model B we assume (Section 2.2.1), that the

dust particles released during sublimation of ice are not transported by the water vapor escaping to space. Dust collected on the surface of the nucleus is removed in a given sector only during events of the blow-out of the whole dust mantle. Thus, as long as the vapor pressure is lower than the threshold value p_{max}, we can geometrically estimate the relation between the ice sublimation rate and the thickening rate of the dust layer. The complete sublimation of ice from the layer of a thickness Δ, results in the formation of dust layer of the thickness Δ_d and the recession of the nucleus surface by $\Delta - \Delta_d$. The relations between those variables depends on the considered material structure. We assume, that the ice grains form matrix the simple cubic structure and the dust grains released during ice sublimation do not change their horizontal positions. In such case geometrical calculations show, that the increase of dust thickness and the dust porosity are:

$$\Delta_d \leq \Delta(v_i/v_m + 1)^{-1/3}, \text{ and } \psi_d \leq 1 - v_m(v_i/v_m + 1)^{1/3}, \tag{10}$$

respectively. The distances between the dust grains in the mantle r_d are in this model determined by the distances between the ice-dust grains, hence on the pore radius r_p in the medium beneath the dust mantle. The relation depends on the relative contents of ice and dust. For the values considered in this paper $r_d \sim 2r_p$. Here v_i and v_m are the dimensionless volumes of icy and mineral components in the comet nucleus. When we assume the porosity of the ice-dust medium $\psi = 0.5$, and the volumetric proportion of ice to dust $f_i : f_d = 2.7175$ in compacted material, as considered by Davidsson et al. (2007) as most appropriate for comet Tempel 1, we obtain $v_i = 0.3655$ and $v_m = 0.1345$. Correspondingly, we get $\Delta_d \leq 0.65\Delta$ and $\psi_d \leq 0.8$. This estimate is very rough, but matches the results of more complex studies. The

dust aggregates formed due to the ballistic particle-cluster aggregation should have the porosity 0.85 (Kozasa et al., 1992). The laboratory simulations of this process performed recently by Blum et al. (2006) gave the porosity $\psi_d = 0.63 - 0.85$ for the spherical particles and $\psi_d = 0.80 - 0.93$ for irregular ones. The lowest limit for the porosity results from the consideration of the random close packing. For the monodisperse spherical particles $\psi_d = 0.365$ (Torquato et al., 2000). The porosity of the dust mantle is related to its dimensionless density v_d by $\psi_d = 1 - v_d$. In our work we consider $\psi_d = 0.73$ as our canonical value, but we test also $\psi_d = 0.36$. For the ratio Δ_d/Δ, above estimated to be lower than 0.65, we assume the value 0.5. This means, that the recession of the ice-dust interface by 1 cm implies increase of the dust thickness by 0.5 cm. For the characteristic radius of the pores r_d in dust mantle we consider four values: 0.025, 0.05mm, 0.1mm and 0.5mm. In Figs. 3,4, and 5 we demonstrate roles of r_d, ψ_d, and $r_p = r_g$. In this part of our considerations those parameters are independent. Further, $r_d = 2\,r_p$, and $v_d = 0.27$ ($\psi_d = 0.73$).

The thermal conductivity λ_d can be calculated using the thermal inertia I_t, derived from the IR observations of the cometary surface. A'Hearn et al. (2005) have found that the maximum temperature corresponds to the area close to the subsolar point and is very high, 326 ± 6 K. They conclude, that the thermal inertia is probably $I_t < 100$ Ws$^{1/2}$K^{-1}m^2. If the dust mantle is thicker than the diurnal thermal skin, the value of I_t derived by A'Hearn et al. (2005) reflects properties of the dust mantle. In such case, knowledge of the dust density ϱ_d and of the specific heat c_d is sufficient to calculate the thermal conductivity λ_d using simple relation $I_t = (\varrho_d c_d \lambda_d)^{1/2}$. The dust layer density is related to the porosity, $\varrho_d = \varrho_{d,bulk}(1 - \psi_d)$, where $\varrho_{d,bulk}$ is the density of material forming dust grains. Thus, when $I_t = 100$ Ws$^{1/2}$K^{-1}m^2, $\varrho_{d,bulk} = 2087$ kg m^{-3}

(Davidsson et al., 2007), $\psi_d = 0.73$ as described above in this section, and $c_d = 1200\ \mathrm{J\,kg^{-1}\,K^{-1}}$ we get $\lambda_d < 15\ \mathrm{mW\,m^{-1}\,K^{-1}}$. When $I_t < 50\ \mathrm{Ws^{1/2}K^{-1}m^2}$ (Lisse et al., 2005a; Groussin et al., 2007) we get $\lambda_d < 4\ \mathrm{mW\,m^{-1}\,K^{-1}}$. For comparison, (Davidsson et al., 2007) considered $\lambda_d = 30\ \mathrm{mW\,m^{-1}\,K^{-1}}$. Finally, in the current work we present simulations for $\lambda_d = 0 - 30\ \mathrm{mW\,m^{-1}\,K^{-1}}$.

The threshold vapor pressure p_{max}, yielding blow-out of the dust mantle, is weakly constrained. Cohesivity of the layer composed of pure dust was analyzed by several authors. According to the review presented by Kührt and Keller (1994), the strength can be $10^2 - 10^4$ Pa. However, the critical is the bounding between the dust mantle and the underlying material. This parameter was not directly measured, but we can constrain it using results of the Deep Impact mission. Observations of the comet Tempel 1 after the impact event show, that the ejecta cone remained attached to the surface of the nucleus. Thus, according to A'Hearn et al. (2005) formation of the crater was not controlled only by the gravity, hence the shear strength of the material around the rim of the crater should be below 65 Pa. This value describes only average properties of the material. It is possible, that just beneath the dust exist some more cohesive layer, while at larger depth material is even weaker. Thus, in our work we consider $p_{max} = 0.5 - 60$ Pa. These values are below the lower limit 100 Pa predicted for dry dust. However, dust layer on the subliming ice may behave different than in other conditions (Gruen et al., 1989; Kochan et al., 1990). During Cometary Simulations Experiments KOSI authors observed significant vibrations of the dust particles at the surface of samples. They argue, that those vibrations may enhance ability of the dust particles to leave the dust layer. We suppose also, that the vibrations can be particularly important when the dust particles are fluffy agglomerates of smaller grains.

Such structures may be easily destroyed. If vibrations are not restricted to the surface, they could significantly reduce strength of the whole dust mantle.

Albedo of the dust covered surface is $A_d = 0.03$. When the dust mantle is blow out albedo of the surface remains unchanged.

3.2 Material underlying the dust mantle

In our model structure of the nucleus material underlying the dust mantle is described by two variables and three constants. Variable are the porosity ψ, and the Hertz factor h, while the radii of the grains and the pores $r_g = r_p$, and the tortuosity of the pores are constant. The tortuosity is $\tau = \sqrt{2}$, and $r_g = r_p = 0.01 - 0.100$mm. The initial value of the Hertz factor is $h_0 = 0.001$. The porosity is expressed by $\psi = 1 - v_m - v_i$, where v_m is constant, but v_i slowly increases from the initial value v_{i0}. In our work $v_m = 0.1345$ and $v_{i0} = 0.3655$. They combine to the density $\varrho = 620\ \mathrm{kg\,m^{-3}}$. This value was used by A'Hearn et al. (2005). Other authors obtained for comet Tempel 1 lower bulk densities $\varrho = 450 \pm 250\mathrm{kg\,m^{-3}}$ (Davidsson et al., 2007) and $\varrho = 400 \pm 300\mathrm{kg\,m^{-3}}$ (Richardson and Melosh, 2006).

In reality, radii of the grains and the pores can slightly change as the migrating vapor condenses. However, these changes are not so significant as the changes of grain-to-grain contact areas resulting from the activity of sintering mechanisms. When the porosity locally increases from $\psi_0 = 1 - v_m - v_{i0}$ to $\psi = 1 - v_m - v_i$, the effective pore radius should become $r_p(v_i) \sim r_p(1 - (v_i - v_{i0})/(1 - v_m - v_{i0}))^{1/2}$. When $v_m = 0.1345$ and the volume of ice increases from $v_{i0} = 0.3655$ to $v_i = 0.5155$, that reduces porosity by 30%

from 0.5 to 0.35. In this case, the effective pore radius should decrease only by about 16%. Our simulations show, that v_i are always below 0.4. Thus, porosity does not change by more than 10% and r_p by just few percent. At the same time, the Hertz factor can increase from 0.001 to 0.34 down to some meters below the ice/dust interface. Profiles of the Hertz factor versus depth and their correlation with the temperature profiles are discussed in the Section 5.2.

3.3 Orbit, shape, and orientation

The comet nucleus is assumed to be a prolate ellipsoid, with large semi-axis $a = 3800$ m and short semi-axes $b = c = 2450$ m (A'Hearn et al., 2005). The rotation axis is along the maximum moment of inertia, thus the comet nucleus rotates about one of its short axis. We apply the rotational period $P_{rot} = 40.74$ hours and the orientation of the spin axis determined by Belton et al. (2006). They found the positive spin pole to be at RA = 293.8^o, DEC = 72.7^o, with an uncertainty of 5^o. More recently Thomas et al. (2007) uses RA = 294^o, DEC = 73^o In the orbital plane coordinates employed in our paper the spin axis orientation corresponds to $(I, \phi) = (11.5^o, 53.8^o)$, where the angle I is the obliquity of the orbital plane to the cometary equator and the angle ϕ is the solar longitude at perihelion, measured from the vernal equinox of the comet in the sense of increasing true anomaly. Orbit of the comet is represented by the orbital elements corresponding to the last apparition in 2005. Thus, we have eccentricity $e = 0.517491$, perihelion distance $q = 1.506170$ AU and the orbital period $P = 5.515$ years. We have decided not to consider changes of the orbital elements, because comet Tempel 1 has currently very stable orbit. During past 30 years orbital elements remained constant with the accuracy of 1%. So small

changes can not have detectable influence on the water production curve, that is derived from observations with the accuracy of one order of magnitude.

4 Observational data

In our analysis the activity profiles of comet 9P/Tempel 1 are represented by the observed water production rate and the visual light curve for the last apparition in 2005. The photometric data of the comet are taken from International Comet Quarterly archive of photometric data, in electronic form (Green, 2005). The total number of magnitude estimates made by 63 observers amounted to 639, spanning a period from January 2005 to October 2005. We corrected the data for the geocentric distance to derive heliocentric magnitudes as a function of time from perihelion. Due to a large scatter ($\sim 2^{mag}$) of the magnitudes we decided to use estimates made by more experienced observers. Finally, in total, 18 observers and 265 observations we selected for analysis. We have chosen observers which observations are internally consistent. As it is known the apparent brightness depends on the instrument used to view it as well as on individual observers. We derived the observers specific corrections comparing observations made within two days with different observers and telescope types. In general larger corrections are associated with larger telescope apertures. The observations made with small instruments do not need corrections. The detailed list of corrections will be publish elsewhere together with the brightness curves for others apparitions of the comet. The corrected heliocentric magnitudes are finally converted into water production rates using the commonly used empirical law: $logQ_{H_2O} = C - 0.24\ m_H$ (e.g. Jorda *et al.* (1992)). We have found the coefficient $C = 30.57$ by comparing

the levels of the visual light curve given by m_H and the observed water production rate. The latter is represented by five sets of measurements provided by Mumma et al. (2005) (ground-based infrared spectroscopy), Bensch et al. (2005) (Submillimeter Wave Astronomical Satellite), Mäkinen et al. (2007) (SWAN- Lyman alpha), Schleicher (2007) (narrow band photometry), and Biver et al. (2007) (Odin; OH observations at Nancay). In the latter case the OH production rates were converted into water production, assuming that $Q_{H_2O} = Q_{OH}/0.89$. Observed water production rates versus time to perihelion are shown in Figs.7, 8, 13, by big symbols. In the same figures water production derived from brightness measurements are marked with dots. The comet brightness features a slight asymmetry close to perihelion with a peak about 20 days before perihelion. However, the activity seems to be enhanced over 3-4 weeks. As we have checked the visual light curves for three last apparitions in 2005, 1994 and 1983 seem to be consistent in their profiles i.e. they are more steeper before perihelion than in the post-perihelion branch. Furthermore, the production peak is currently a bit closer to perihelion than in the older apparition and the level of water production in 1983 was clearly higher than in 2005. The maximum value of water production in 2005 was about $1.1 \cdot 10^{28}$ mol./s, and in 1983 amounted to about $2 \cdot 10^{28}$ mol./s. Comparisons of the 1983 and 1994 apparitions made by Lisse et al. (2005b) also showed the factor of 2 decrease in the production rate of water from 1983 to 1994. According to Schleicher (2007) by 2005 water production rate decreased to only about 42% of its 1983 values. The variation of outgassing within the last apparitions is unexpected taking into account the lack of significant perturbations of the comet's orbit, so the pattern of insolation is the same in each return of the comet to the Sun and different possibly active regions are illuminated in the same way. Thus, the most likely explanation for the changes of water

production are some changes of the dust mantle.

5 Results, constant thickness of the dust layer - Model A

5.1 Water production

The simulations are started when the comet is at aphelion, hence the surface is uniformly cold. We have usually run three or four orbital revolution of the comet with a fixed spin axis orientation. In this section we present results obtained, when we assumed constant thickness of the dust mantle, either uniform, or not.

5.1.1 Uniform dust mantle

In Fig. 3 we show influence of the dust thickness, when it is uniform, on the total water production from the nucleus. The dust layer has the thermal conductivity $\lambda_d = 20$ mW m^{-1} K^{-1} and its thickness is either 1cm, or 4cm. It can be seen, that the calculated profile of water production versus time initially changes from one perihelion to the next one before the initial conditions are forgotten. Thickness of the dust mantle has strong influence on the number of orbital periods before the seasonal cycle of water emission becomes stable. When the dust is only 1 cm thick, stable cycle is established already after one orbital period, while for the 4 cm thick dust layer are needed eight orbital revolutions. The time, when water emission reaches its maximum also depends on the dust thickness, it falls roughly at perihelion when the dust is 1cm thick, but about 40 days later when the dust thickness is 4 cm. More interesting is,

how the value of seasonal maximum depends on the dust thickness. When the dust is only 1cm thick, peak value of water emission from the nucleus is one order of magnitude higher than observed. In contrary, when the dust layer is 4cm thick, the peak value of water production is one order of magnitude too small. It is important, that the moderate change of the dust thickness results in the very strong change of the water production. The ratio between the calculates seasonal peaks is after several orbital periods about 140. This is due to nonlinear dependence of the sublimation rate on the temperature T_{int} beneath the dust mantle. The value of T_{int}, and hence the rate of sublimation, depends on the balance between the heat flux conducted through the dust mantle F_{mantle}, heat flux F_{down} conducted from the sublimation front downward to the interior of the nucleus, and the flux of energy F_{subl} consumed during sublimation of ice. When the dust mantle is thin and hence F_{mantle} is high, $F_{mantle} \sim F_{subl}$. As the dust thickness increases resulting in a decrease of F_{mantle}, the relative role of cooling flux F_{down} increases and finally flux F_{subl} becomes minor component in the balance. Concluding, according to our simulations thickness of the dust mantle has very important influence on the water production, but the actual vapor flux should significantly depend also on the medium underlying the dust mantle. Most important, simulations with uniform dust mantle can not reproduce together the value and the time of the observed seasonal maximum of water production.

In Fig. 4 we show, how granulation of the material affects water production curve. The simulations were performed assuming size of pores in the dust mantle independent on the pore sizes beneath the dust. The porosity of the dust mantle is $\psi = 0.73$ ($v_d = 0.27$). The radius of pores r_d is within the range 0.05 - 0.50 mm, while the effective radius of pores r_p beneath the dust layer

is 0.025 - 0.200 mm. The role of pore radii in the dust mantle is significant, but smaller than it could be expected. The increase of r_d from 0.05 - 0.50 mm enhances water production at perihelion 3.8 times. This factor is lower than the factor 10, suggested by the Eq. 2. This is because any increase of vapor emission enhances cooling of the medium (Eq. 8) and hence reduces the rate of sublimation. The rate of sublimation is proportional to the saturation vapor pressure, that is exponential function of temperature. This makes relation between the water production and the pore radius r_d strongly nonlinear. The role of $r_p = r_g$ significantly depends on the dust thickness. When the dust layer is only 1 cm thick, granulation of the medium beneath the dust mantle affects water production only before perihelion in a moderate way. When $r_p = 0.20mm$,the total flux of water emitted 150 days before perihelion is 1.5 times larger than calculated assuming $r_p = 0.05mm$. At perihelion the difference becomes negligible. When the dust layer is 4 cm thick, influence of r_p is prominent at any time. Finally, we have found that: the role of pore sizes in the dust layer is significant, but smaller than it can be expected, and that the granulation of the medium beneath the dust can be either significant, or not, depending on the thickness of the dust layer.

In Fig. 5 we show influence of the density, or porosity, of the dust mantle on the water production curve. The dust mantle has thickness of 1 cm, and the radii of pores are: $r_d = 0.10$ mm, and $r_p = r_g = 0.05$ mm. The dimensionless density of the dust mantle v_d is either 0.27, or 0.64. These values correspond to the porosity ψ_d equal to 0.73, and 0.26. The ratio between the dust densities is 2.8, while the difference of the water production maximum is about 1.8. Thus, porosity of the dust mantle has influence on the emission of water. However, the same as we found for the pore radius r_d, the influence is smaller than it is

suggested by the proportionality in Eq. 2.

In Fig. 6 are shown profiles of water emission versus time for 8 sectors of the nucleus surface. The selected sectors cover one quarter of the nucleus, for latitudes within the range from -90^o to$+90^o$. The dust layer is 1cm thick, $r_p = 0.05$ mm, $r_d = 0.10$ mm, and $\psi_d = 0.73$. The profiles are drawn for the second perihelion passage covered by our simulations. The results for consecutive perihelions are almost the same and are not plotted. It can be seen, that in most cases profiles have the same shape with maximum close to perihelion. Only at middle and high latitudes in the south hemisphere maximum of sublimation falls before perihelion, by 40 and 70 days respectively. Low sublimation from the sector centered at the latitude -60^o may be related to unfavorable illumination. For this sector zenithal angle is always high and has minimum well before perihelion, when the nucleus is still very cold. For the remaining sectors the seasonal peak of water production is shifted relative to perihelion by less than 30 days. Small differences between most profiles are not surprising, because at small obliquity of the nucleus seasonal effects should not be prominent. However, small time shifts of the seasonal maximum of sublimation appear essential for the agreement between the calculated profiles of total water emission from the nucleus and the observed one, that is not symmetric relative to the perihelion.

5.1.2 Non-uniform dust mantle

In Fig. 7 we show water production from the nucleus versus time, calculated when ice can sublime effectively only from two sectors of the nucleus surface. They are centered at the latitude -21^o, at two different longitudes among

four that are analyzed in the model with 32 sectors. In the selected two sectors, the dust layer is only 1 cm thick, while the remaining surface of the nucleus is covered by thick isolating dust mantle. The remaining parameters are: $r_p = 0.05$ mm, $r_d = 0.10$ mm, $\psi_d = 0.73$, and $\lambda_d = 20$ mW m^{-1} K^{-1}. The simulated profile matches observations. The exception is the post-perihelion branch where the number of data points available for the recent apparition in the year 2005 is small and exhibits rather high scatter, making observational profile uncertain. Our current analysis of the dust properties is based on the near perihelion part of the orbital period, when the sublimation is strongest. For this period, agreement between the calculated and observed water production requires restriction of the sub-dust sublimation to two selected areas in the south hemisphere, at the latitude about -20^o, hence about 30 degrees south of the subsolar latitude at perihelion. Each of these active sectors covers only about 3% of the nucleus surface. Thus, they are not large, but could be visible if any of them is in the half of the nucleus imaged by Deep Impact spacecraft. The expected temperature contrasts will be discussed in the Section 5.2.

The above presented solution for the distribution of dust thickness, yielding agreement between simulated and observed water production, is not unique. We have found profiles similar to those shown in Fig. 7 also when the dust mantle in the active regions is thicker than 1 cm. In Fig. 8 we show results of calculations for the nucleus with active areas covered by thicker dust, now 2cm, and occupying larger fraction of the nucleus surface. Grain size is now larger, $r_g = 0.1$ mm. Two active sectors are centered at the latitude -12.0^o, four at -21^o and four the latitude -30.2^o. Together they occupy about 30% of the nucleus surface. It is important, that again the effective sub-dust sublimation of ice should be restricted to the areas located significantly south of

the subsolar latitude at perihelion. Otherwise, seasonal maximum of the total water emission from the nucleus is delayed when compare to the observed one.

In this, and previous paragraphs we shown, that the observed water production curve can be reproduced when most of the nucleus surface is covered by thick dust layer and ice sublimes only in some regions covered by the thin dust mantle of moderate thermal conductivity about $20\mathrm{mW\,m^{-1}\,K^{-1}}$. Activity of the nucleus must be concentrated in the southern hemisphere. When the active regions are covered by 1 cm thin dust, they should occupy 6% of the surface, while when covered by 2 cm thick dust they should occupy already 30% of the surface. Thus, the former variant with 6% active surface seems more likely and will be further considered as the best one.

5.2 Surface temperature

Comparison of the calculated water production curve with the observations is not only one method of model verification. Before the cratering experiment of the Deep Impact mission the surface of comet Tempel 1 was observed with high resolution, sufficient to construct temperature map. About 20 min before impact 90% of the visible nucleus surface was imaged with the resolution about 200m/pixel (A'Hearn et al., 2005). The temperature derived from observations varies from 260 ± 6 K in the areas illuminated at high zenithal angle to 329 ± 8 K in the subsolar point (A'Hearn et al., 2005; Groussin et al., 2007). Unfortunately, derived map of surface temperature is only for one fixed time, so the temperatures at different points correspond to the different local times and hence different illumination angles. This is not sufficient to distinguish dependence of the surface temperature on the topography dependent illumi-

nation, on the surface roughness, and the nonuniformity of the dust mantle properties. Thus, in the following we focus our attention on the subsolar temperature and the temperature in the active regions discussed in the Section 5.1.2.

In Fig. 9 we show diurnal changes of the surface temperature in the selected location at the latitude -21^o, hence in one of the two active sectors predicted by our best model (Fig. 7). In addition to the profile for the dust layer of the thickness 1 cm and the thermal conductivity 20 $\mathrm{mW\,m^{-1}\,K^{-1}}$, we drown profile for the very thick and extremely low conducting dust mantle. The day time temperatures differ by less about 20 K. Thus, the temperature contrast between the active area covered by thin dust mantle and the surrounding terrain should be visible on a smooth hypothetical nucleus, but probably not on the real one with complex topography. For comparison, active area covering 30% of the nucleus (Fig. 8) should be visible if it exists. Therefore, we can conclude that our model with active 6% of the nucleus surface, covered by 1 cm thick dust passed double test: comparison of the simulated and observational water production curves, and the temperature test. The temperature of the active sectors is above the minimal temperature observed by Deep Impact.

To discuss dependence of the subsolar temperature on the dust mantle properties we selected within our latitude-longitude grid one sector $(12^oN, 10^oE)$ (longitude recalculated to the grid used by Thomas et al. (2007)). This sector is at the latitude almost the same as the point $(10^oN, 330^oE)$ being subsolar at the time of the observations. Closer match of the longitude seems not necessary because we do not consider role of the topography. For the selected location we analyzed the diurnal changes of the calculated temperature to find its maximum. In Fig. 10 we show profiles of temperature versus depth

for different thicknesses of the dust layer. The dust has thermal conductivity $\lambda_d = 20$ mW m^{-1} K^{-1} and the pore radii $r_d = 0.10$mm. In the underlying medium $r_g = r_p = 0.05$mm. The profiles are drawn for the third perihelion passage covered by our simulations. It can be seen, that the profiles have steep like character with nearly flat part immediately beneath the dust mantle. This part extends up to four meters below the surface, hence to the lower boundary of the strongly sintered layer that forms beneath the dust mantle as is shown in Fig. 11. It can be seen, that beneath the 1 cm thick dust mantle forms cohesive layer of sintered grains about 2 m in thickness. Beneath 2 cm of dust cohesive layer is almost two times thicker. Further increase of the dust thickness did not result in any thickening of the cohesive layer. However, sintering under thick dust is slower due to lower temperature. Hence, for the thickest dust quasi-steady state was still not reached.

The surface temperature significantly depends on the dust thickness when the dust is thin. When the dust has thickness 1cm, the peak value of the surface temperature in the selected point is about 301K. This value is roughly 30K lower than the observed subsolar temperature. When the dust thickness is 4 cm instead of 1 cm, the temperature in the nearly subsolar sector becomes about 313K, about 12 K higher but still about 15K too low. Reducing thermal inertia of the dust mantle from 100 W s$^{1/2}$ K^{-1} m^{-2} to 5 W s$^{1/2}$ K^{-1} m^{-2} together with the increase of the dust thickness to 40 cm results in the increase of the surface temperature in the subsolar point to 321K. This value is already close to the observed one. This indicates, that presence of thick dust layer of very low thermal inertia, is required to reproduce observed surface temperature. Similar effect was found by (Groussin et al., 2007), whose simulations properly reproduced observations only when the thermal inertia of the medium was

zero. Such thick and low-conducting dust mantle effectively disables sub-dust sublimation of ice resulting in zero activity of the comet, that is in contrary to the observations.

Our simulations described in the previous subsection show, that only some small fraction of the nucleus surface should be active, hence covered by thin dust of non-zero thermal inertia. This result removes contradiction between the above described requirements regarding properties of the dust mantle. It should be thick and has extremely low thermal conductivity everywhere except small, 6%, fraction of the surface in the south hemisphere. These active surface can be located either at the imaged side of the nucleus, or at the opposite one.

6 Results, evolving thickness of the dust mantle - Model B

In this section we present simulations including evolution of the dust mantle. It grows in thickness due to the sub-dust sublimation of ice, and episodically can be blown out, as we described in the section 2.2.1. The dust mantle is blown out when the vapor pressure beneath dust exceeds the threshold pressure p_{max}.

6.1 High p_{max}

In Fig. 12 we show calculated water production versus time at three consecutive orbital periods. The dust layer is initially 1.5 cm thick, and $r_d = 0.10$mm. The thermal conductivity of the dust mantle, λ_d is represented by three values 30 mW m^{-1} K^{-1}, 20 mW m^{-1} K^{-1}, and 10 mW m^{-1} K^{-1}. In the material beneath the dust $r_g = 0.05$mm. The threshold pressure $p_{max} = 10$ Pa. In all simulations the dust mantle is never blown out. Thus, it increases in thickness

from orbit to orbit. When $\lambda_d = 30$ mW m^{-1} K^{-1}, the dust mantle significantly increases in thickness only during the first three perihelion passages. The corresponding changes are: 4.5 cm, 1 cm, and 0.5 cm at the latitude $+12^oN$; and 2.5 cm, 1.5 cm, and 0.5 cm, at the latitude $+60.5^oN$. The increasing thickness of the dust mantle results in a decrease of water production from the nucleus, that independently on λ_d quickly becomes much smaller than the observed one. In addition, we have found, that the calculated water profiles have too late maximum. The results of simulations presented in this paragraph indicate, that the threshold pressure allowing local blow-out of the whole dust needs to be lower than 10Pa. This requires some mechanism reducing cohesivity below that expected for dry dust under static conditions, as we discussed in Section 2.2.1.

6.2 Low p_{max}

In Fig. 13 we show results of calculations performed assuming very low threshold pressure $p_{max} = 1$ Pa. The initial dust thickness is: everywhere 1.5cm (upper panel), or 1.5 cm in 3 sectors (1 at -21^o, and 2 at 30^o) and 10 cm on the remaining surface (lower panel). The remaining parameters are: $r_g = r_p = 0.01$ mm, $r_d = 0.05$ mm, and $\lambda_d = 30$ mW m^{-1} K^{-1}. The values were chosen after several test simulations. In the case of initially uniform dust mantle the calculated profile of water production versus time clearly does not match observations, while in the latter agreement is satisfying.

When the dust is initially uniformly thin, it is periodically blown out close to perihelion everywhere except high latitudes in the south hemisphere. After blown out of the dust mantle surface quickly covers by dust released due

to sublimation of ice mantling cometary grains. However, sublimation of an uncovered ice, and beneath thin dust is very fast and almost everywhere on the nucleus the dust becomes blown out again in the same day. Close to perihelion, the dust is blown out as soon as the dust thickness reaches size of the numerical cell and our program can calculate the vapor pressure beneath the dust. Thus, the dust thickness remains very small. Only when the flux of solar energy becomes too low for the vapor pressure to remain above p_{max}, at low latitudes about 150 days after perihelion, the dust mantle starts to grow in thickness. However, at that time solar flux is already low and the dust thickness does not increase to more than 1 cm before the activity becomes negligible. Before the consecutive perihelion passage the vapor pressure starts to rise and the dust is blown out again, at low latitudes about 200 days before perihelion. Therefore, in the period from -200 to 150 days with respect to perihelion (the heliocentric distance smaller than about 2 AU), large fraction of the nucleus surface is covered by very thin dust layer. This reduces day time warming of the surface. The uncovered, or nearly uncovered surface warms up only to the temperature about 200 K, much lower than observed and much lower than predicted by the Model A. Thus, the model with initially uniform dust is not appropriate. It does not reproduce observed water production, as we already found when we performed simulations using Model A, and predicts very low surface temperature.

When the dust is thin only in the selected regions (lower panel of Fig. 13), hence the surface is only partially active, the calculated water production from the nucleus matches observations. Unfortunately, close to perihelion the calculated thickness of the dust mantle is in the active areas very small, as already described in the previous paragraph. Thus, about 10% of the surface

should have temperature about 200 K, while the temperature derived from observations is above 260K everywhere at the illuminated side of the nucleus (A'Hearn et al., 2005). It should be noted, that the cohesity required for the dust to be blown out is very low. The dynamical character of the process we suggest as responsible for reducing dust cohesity may indicate, that the dust mantle becomes sufficiently low cohesive only episodically. If so, our Model B is applicable to describe outburst events.

Finally, after performing our double stage verification we can conclude that model with constant thickness of the dust mantle, our Model A, is appropriate for comet 9P/Tempel 1, while the Model B with episodically blown out dust mantle predicts far too low temperature of large fraction of the nucleus surface.

7 Summary and conclusions

In the current work we attempted to answer the question: what are the properties of the dust mantle of comet 9P/Tempel 1?. Our aim was to determine the thermal inertia of the dust cover and the large scale distribution of the dust thickness. For this purpose we compared the simulated and observational profiles of the water production from the nucleus versus time. We have also performed second stage of model verification, to our knowledge not applied before to any complex model of a comet nucleus. We compared the calculated and observed surface temperature in the subsolar point at perihelion.

We have performed several simulations, using models with dust mantle of the thickness either constant, both uniform and nonuniform (Model A), or evolving (Model B). The former model assumes fixed properties of the dust

layer like porosity and pore radius as well as its constant thickness. We have studied the influence of the size of grains and pores as well as the thickness of the dust cover on the water production rate. We have also analyzed possible evolution of the dust mantle. In the Model B the dust mantle increases in thickness until the vapor pressure beneath the dust exceeds the threshold value and the whole dust mantle is locally blown-out.

The Model A with constant, but non-uniform thickness of the dust mantle predicts, that 94% of the nucleus surface should be covered by very thick and extremely low conducting dust mantle. On the remaining 6% of the surface the dust should be 1 cm thick and have relatively high thermal inertia about 100 $\mathrm{W\,s^{1/2}\,K^{-1}\,m^{-2}}$. This active area should be located in the southern hemisphere, about 30^o south of the subsolar latitude at perihelion. The Model A properly reproduces the observed water production curve and predicts surface temperature matching observations.

The Model B predicts, that about 10% of the nucleus should be periodically active. Close to perihelion the active surface should be uncovered, or covered by the dust cover no more than few millimeters thick. Thus the temperature is higher than the minimal temperature on the thermal maps of the comet nucleus. At aphelion the dust mantle is in the active regions about 1 cm thick. Before perihelion the dust mantle grows to 2 cm before it is blown out. For a given location the seasonally averaged dust thickness predicted by the Model B is about 1 cm. This matches the dust thickness predicted for the active regions by the Model A.

The presented simulations show, that: (i) both models can reproduce general shape of the observed water production curve from comet Tempel 1, but

(ii) the agreement of the calculated surface temperature with observations is satisfying only in the case of Model A.

The difference of the thermal predictions of two models equally well reproducing the observed water production curve indicates high importance of the double stage model verification procedure, wherever the temperature observations are available. This indicates also, that observations of the surface temperatures of cometary nuclei are very important to understand their structure and evolution.

References

A'Hearn, M. F., Belton, M.J.S., Delamere, W.A., 31 colleagues, 2005. Deep Impact: Excavating Comet Tempel 1. Science 310, 258-264.

Belton, M. J. S., Thomas, P. C., Carcich, B., Crockett, C. J., Deep Impact Science Team, 2006. The Spin State of 9P/Tempel 1. LPI37.1487B

Brin, G.D., and Mendis D.A, 1979. Dust release and mantle development in comets. Astrophys. J.229, 402-409.

Bensch, F., Melnick, G.J., Neufeld, D.A., Harwit, M., Snell, R.L., Patten, B.M., 2005. SWAS observations of Comet 9P/Tempel 1 and Deep Impact. In: Lis, D.C., Blake, G.A., Herbst, E. (Eds.), Astrochemistry Recent Succes and Current Challenges, IAU Symposium, vol. 231. Cambridge Univ. Press, Cambridge, pp. 133-134.

Biver, N., Bockelee-Morvan, D., Boissier, J., Crovisier, J., Colom, P., Lecacheux, A., Moreno, R., Paubert, G., Lis, D.C., Summer, M., 7 colleagues, 2007. Radio observations of Comet 9P/Tempel 1 before and after Deep Impact. Icarus 187, 253-271.

Blum, J., Schräpler, R., Davidsson B.J.R., Trigo-Rodriguez, J.M., 2006. The Physics of Protoplanetesimal Dust Agglomerates. I. Mechanical Properties and Relations to Primitive Bodies in the Solar System. Astrophys. Space Sc.652, 1768-1781.

Davidsson, B.J.R., Gutierrez, P.J., Rickman, H., 2007. Nucleus properties of the Comet 9P/Tempel 1 estimated from non-gravitational force modeling. Icarus 187, 306-320.

Eluszkiewicz, J., Leliwa-Kopystyński, J., Kossacki, K.J., 1998. Metamorphism of Solar System Ices. In *Solar System Ices* (edited by Schmitt B., de Bergh C., and Festou M.), Kluwer Academic Publishers, Dordrecht, The Netherlands, 119 - 138.

Groussin, O., A'Hearn, M.F., Li, J.Y., Thomas, P.C., Sunshine, J.M., Lisse, C.M., Meech, K.J., Farnham, T.L., Feaga, L.M., Delamere, W.A., 2007. Surface temperature of the nucleus of Comet 9P/Tempel 1. Icarus 187, 16-25.

Green, D.W.E., 2005. International Comet Quarterly archive of photometric data, in electronic form (Smithsonian Astrophysical Observatory, Cambridge, MA).

Gruen, E., Benkhoff, J., Fechtig., H., Hesselbarth, P., Klinger, J., Kochan, H., Kohl, H., Krankowsky, D., Lammerzahl, P., Seboldt., W., Spohn, T., Thiel, K., 1989. Mechanisms of Dust Emission from the Surface of a Cometrary Nucleus. Adv. Space Res. 9, 3133-3137

Haruyama, J., Yamamoto, T., Mizutani, H., Greenberg, J.M., 1993. Thermal history of comets during residence in the Oort Cloud: effect of radioactive heating in combination with the very low thermal conductivity of amorphous ice. J. Geophys. Res. 98, 15,079-15,090.

Jorda, L., Crovisier, J. and Green, D.W.E., 1992. The correlation between

water production rates and visual magnitudes in comets. In: Asteroids, Comets, Meteors 1991, eds A. Harris and E. Bowell, Lunar Plan. Inst., pp. 285-288.

Kochan, H., Ratke, L., Thiel, K., Gruen, E., 1990. Particle Emission from Artificial Cometary Surfaces: Material Science Aspects. Proceedings of the 20th Lunar and Planetary Science Conference, 401-411.

Kömle, N.I., Steiner, G., 1992. Temperature evolution of porous ice samples covered by a dust mantle. Icarus 96, 204-212.

Kossacki, K.J., Szutowicz, S., Leliwa-Kopystyński, J., 1999. Comet 46P/Wirtanen: Evolution of the Subsurface Layer. Icarus 142, 202-218.

Kossacki, K.J., Leliwa-Kopystyński, J., Szutowicz, S., 2006. Evolution of depressions on the comet 67P/Churyumov-Gerasimenko: role of ice metamorphism. Icarus 184, 221-238.

Kossacki, K.J., Szutowicz, S., 2006. Comet 67P/Churyumov-Gerasimenko: Modeling of orientation and structure. Planet. Space Sc.54, 15-27.

Kozasa, T., Blum, J., Mukai, T., 1992. Optical properties of dust aggregates. I - Wavelength dependence. Astron. Astrophys.263, 423-432.

Kührt E., Keller, H.U., 1994. The formation of cometary surface crusts. Icarus 109, 121-132.

Lisse, C.M., A'Hearn, M.F., Groussin, O., Fernandez, Y.R., Belton, M.J.S., van Cleve, J.E., Charmandaris, V., Meech, K.J., McGleam, C., 2005. Rotationally Resolved 8-35 Micron Spitzer Space Telescope Observations of the Nucleus of Comet 9P/Tempel 1 Astrophys. Space Sc.651, 139-142.

Lisse, C.M., A'Hearn, M.F., Farnham, T.L., Groussin, O., Meech K.J., Fink, U., and Schleicher, D.G., 2005. The coma of comet 9P/Tempel 1. Sp.Sci.Rev. 117, 161-192

Mäkinen, J.T.T., Combi, M.R., Bertaux, J.-L., Quémarais, E., Schmidt, W.,

2007. SWAN observations of 9P/Tempel 1 around the Deep Impact event. Icarus 187, 109-112.

Mumma, M.J., 13 colleagues, 2005. Parent volatiles in Comet 9P/Tempel 1: Before and after impact. Science 310, 270-274.

Orosei, R., Capaccioni, F., Capria, M.T., Coradini, A., Espinasse, S., Federico, C., Salomone, M., Schwehm, G.H., 1995. Gas and dust emission from a dusty porous comet. Astron. Astrophys.301, 613-627.

Richardson, J.E., Melosh, H.J., 2006. Modelling the ballistic behavior of solid ejecta from Deep Impact cratering event. Lunar Planet. Sci. XXXVII, 1836

Rickman, H., Fernandez, J.A., Gustafson, B.A.S., 1990. Formation of stable dust mantles on short-period comet nuclei. Astron. Astrophys.237, 524-535.

Schleicher, D.G., 2007. Deep Impact's Target Comet 9P/Tempel 1 at Multiple Apparitions: Seasonal and Secular Variations in Gas and Dust Production. Icarus doi: 10.1016/j.icarus.2007.04.013

Sunshine, J. M., A'Hearn, M. F., Groussin, O., Li, J.-Y., Belton, M.J.S., Delamere, W.A., Kissel, J., Klaasen, K.P., McFadden, L.A., Meech, K.J., Melosh, H.J., Schultz, P.H., Thomas, P.C., Veverka, J., Yeomans, D.K., Busko, I.C., Desnoyer, M., Farnham, T.L., Feaga, L.M., Hampton, D.L., Lindler, D.J., Lisse, C.M., Wellnitz, D.D., 2006. Exposed Water Ice Deposits on the Surface of Comet 9P/Tempel 1. Science 311, 1453-1455.

Thomas, P.C., Veverka, J., Belton, M.J.S., Hidy, A., A'Hearn, M.F., Farnham, T.L., Groussin, O., Li, J.-Y., McFadden, L.A., Sunshine, J. M., Wellnitz, D.D., Lisse, C., Schultz, P., Meech, K.J., Delamere, W.A., 2007. The shape, topography, and geology of Tempel 1 from Deep Impact observations. Icarus 187, 4-15.

Torquato, S., Truskett, T. M., and Debenedetti, P.G., 2000. Is Random Close Packing of Spheres Well Defined? PhRvL 84, 2064-2067

Table 1
Location of the sectors on the nucleus surface in the basic nucleus model. The coordinates describe positions of the sector centers.

Latitudes	Longitudes
$\pm 61^o$	47^o, 133^o, 227^o, 313^o
$\pm 30^o$	14^o, 166^o, 194^o, 346^o
$\pm 21^o$	69^o, 111^o, 250^o, 191^o
$\pm 12^o$	31^o, 149^o, 211^o, 329^o

Table 2
Model parameters.

Parameter	Symbol	Units	Value
Emissivity	ϵ		1
Grain/pore radius in the ice-dust medium	$r_g = r_p$	[mm]	0.01 - 0.10
Pore radius in the dust layer	r_d	[mm]	0.025 - 0.50
Thermal conductivity of the dust layer	λ_m	[mW m^{-1} K^{-1}]	0 - 30
Density of the mineral cores of the grains	ϱ_m	[kg m^{-3}]	2078
Thermal conductivity of the mineral cores	λ_m	[W m^{-1} K^{-1}]	3.1
Dimensionless volume of ice	v_i		0.3655
Dimensionless volume of mineral	v_m		0.1345
Thickness of the dust layer (Model A)	Δ_d	[cm]	1 - 40
Albedo	A		0.03
Porosity of the dust layer	ψ_d		0.36, 0.73
Tortuosity	τ		$\sqrt{2}$
Threshold vapor pressure (Model B)	p_{max}	[Pa]	1 - 10
Bulk density of the nucleus	ϱ	[kg m^{-3}]	620
Initial temperature	T	[K]	50
Other parameters			
Nucleus dimensions us	a,b,c	[km]	3.80,2.45,2.45
Rotational period	P_{rot}	[h]	40.74
Obliquity	I	[deg.]	11.5
Solar longitude at perihelion	ϕ	[deg.]	53.8

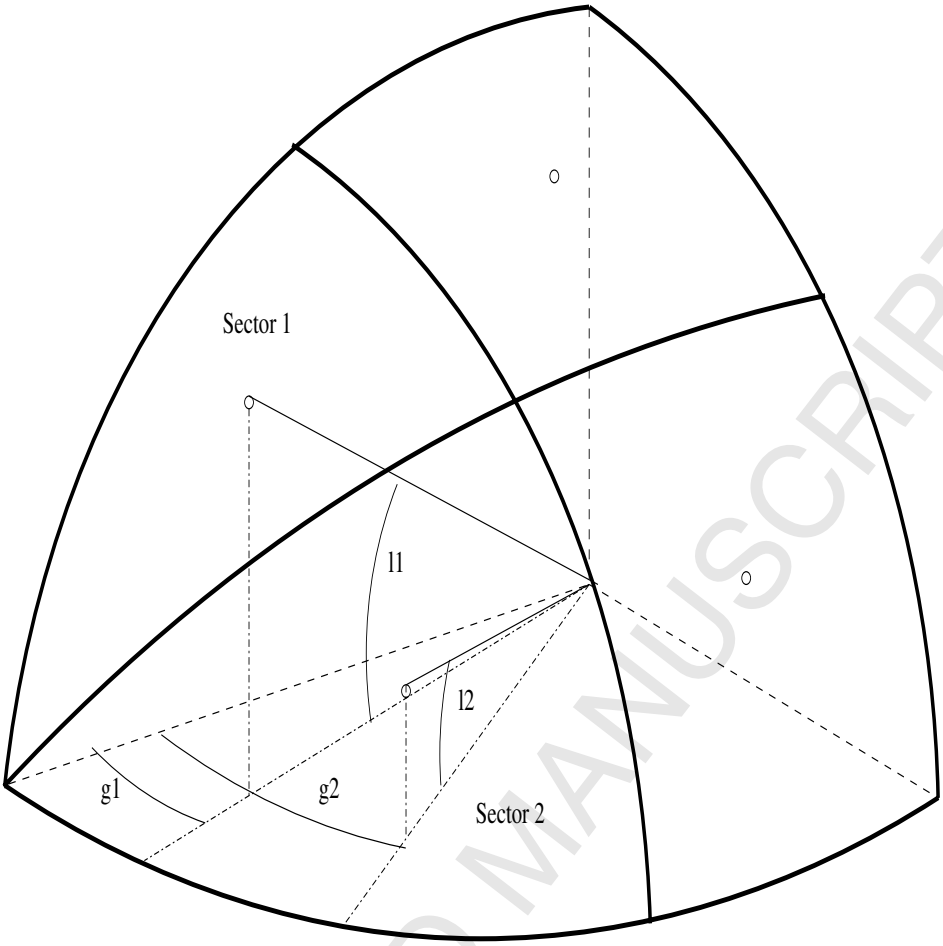

Fig. 1. Sketch of the comet nucleus with marked equal surface sectors considered in the current work. Centers of the sectors are marked by small circles.

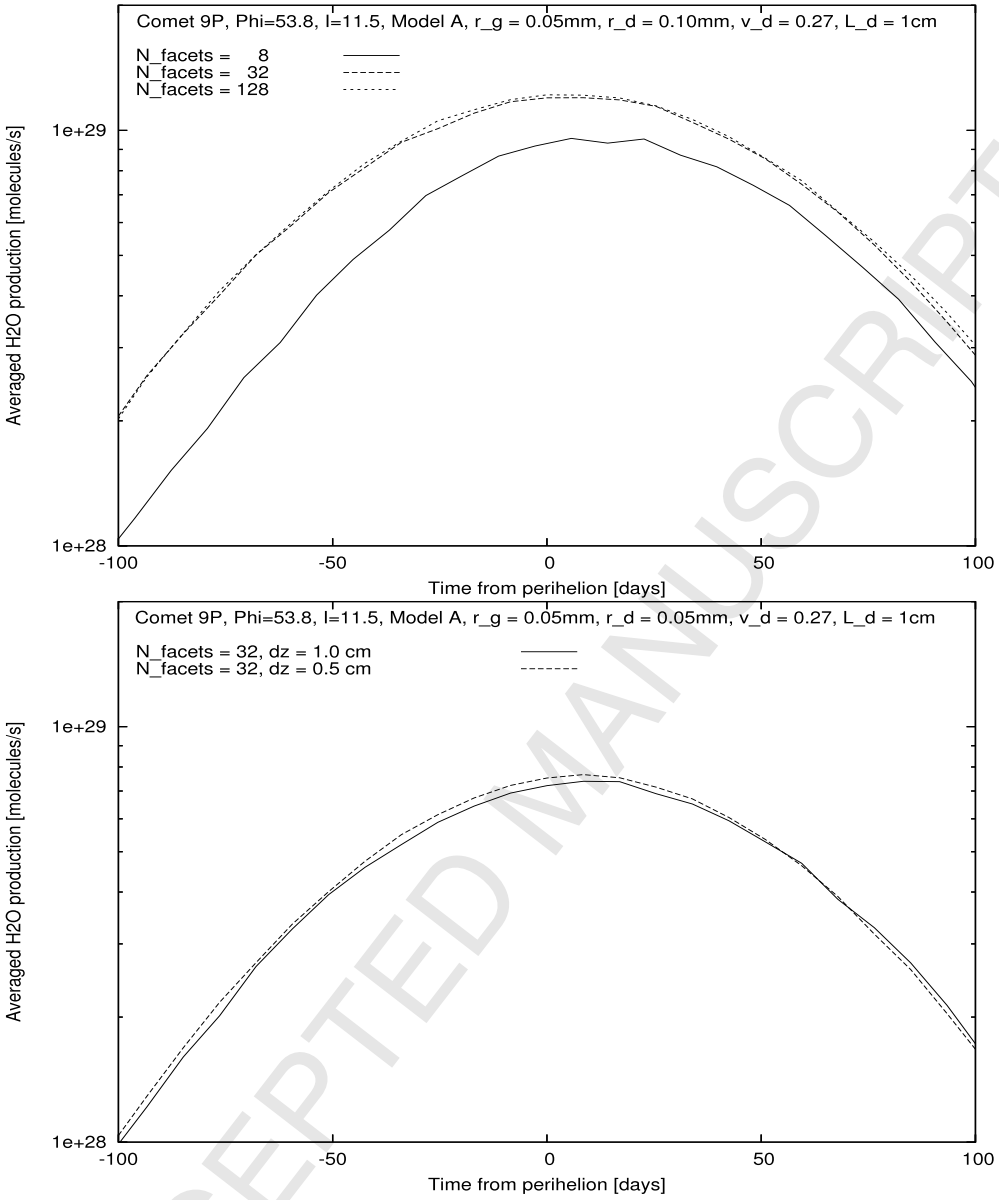

Fig. 2. Role of the resolution. In the figure are shown theoretical water production curves versus time from perihelion, calculated assuming different resolutions (lower panel) and different numbers of facets on the model nucleus (upper panel). The nucleus is composed of the grains with the radii $r_g = 0.05$ mm. Thickness of the dust mantle is constant versus time (Model A). Dust layer has uniform thickness 1 cm, pore radii either 0.1mm, or 0.05mm, and the thermal conductivity $\lambda_d = 20\,\mathrm{mW\,m^{-1}\,K^{-1}}$.

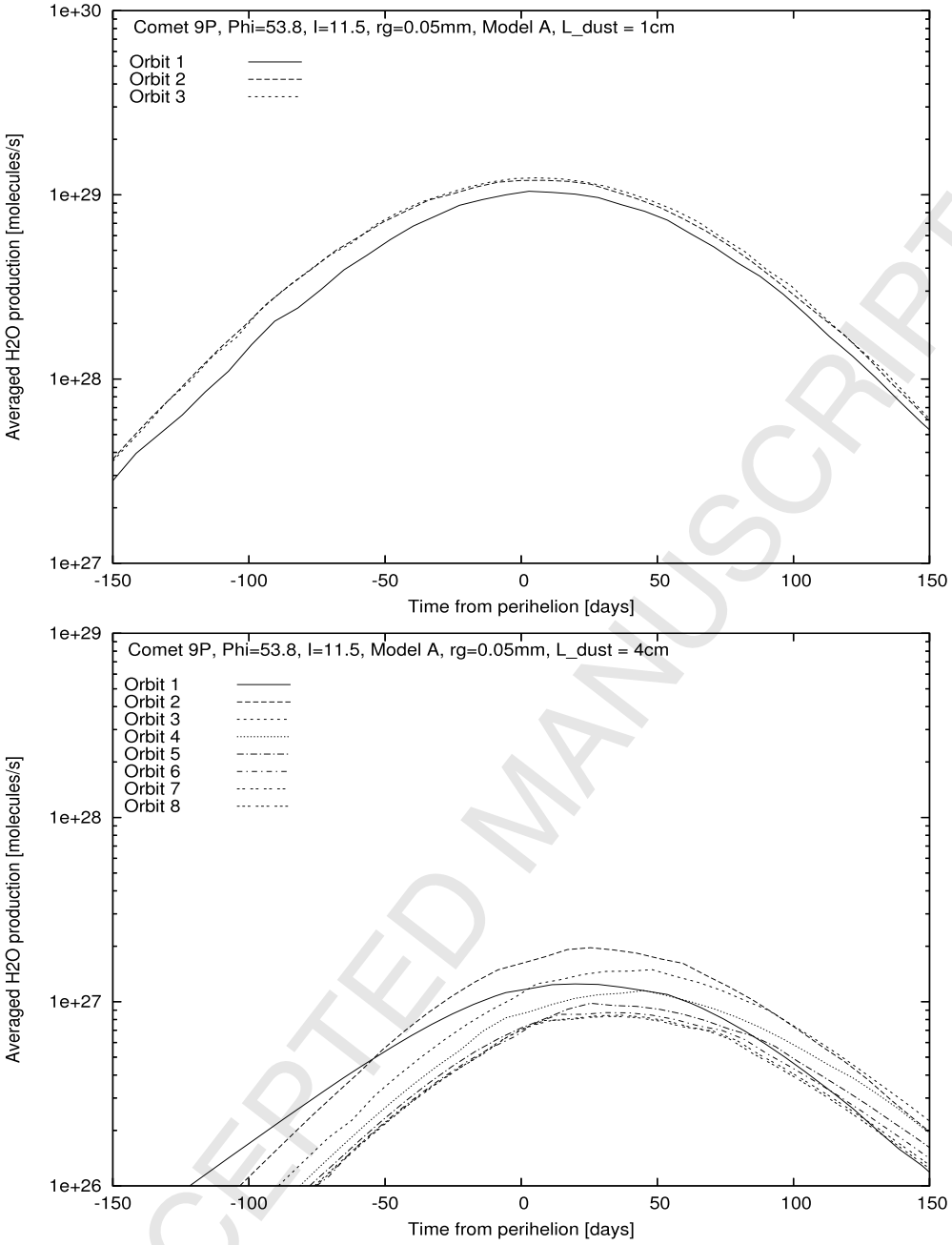

Fig. 3. Theoretical water production curve versus time from perihelion. The nucleus is composed of the grains with the radii $r_g = 0.05$ mm. Thickness of the dust mantle is constant versus time (Model A). Dust layer has thermal conductivity $\lambda_d = 20\ \mathrm{mW\,m^{-1}\,K^{-1}}$ and uniform thickness: 1 cm (upper panel), or 4 cm (lower panel).

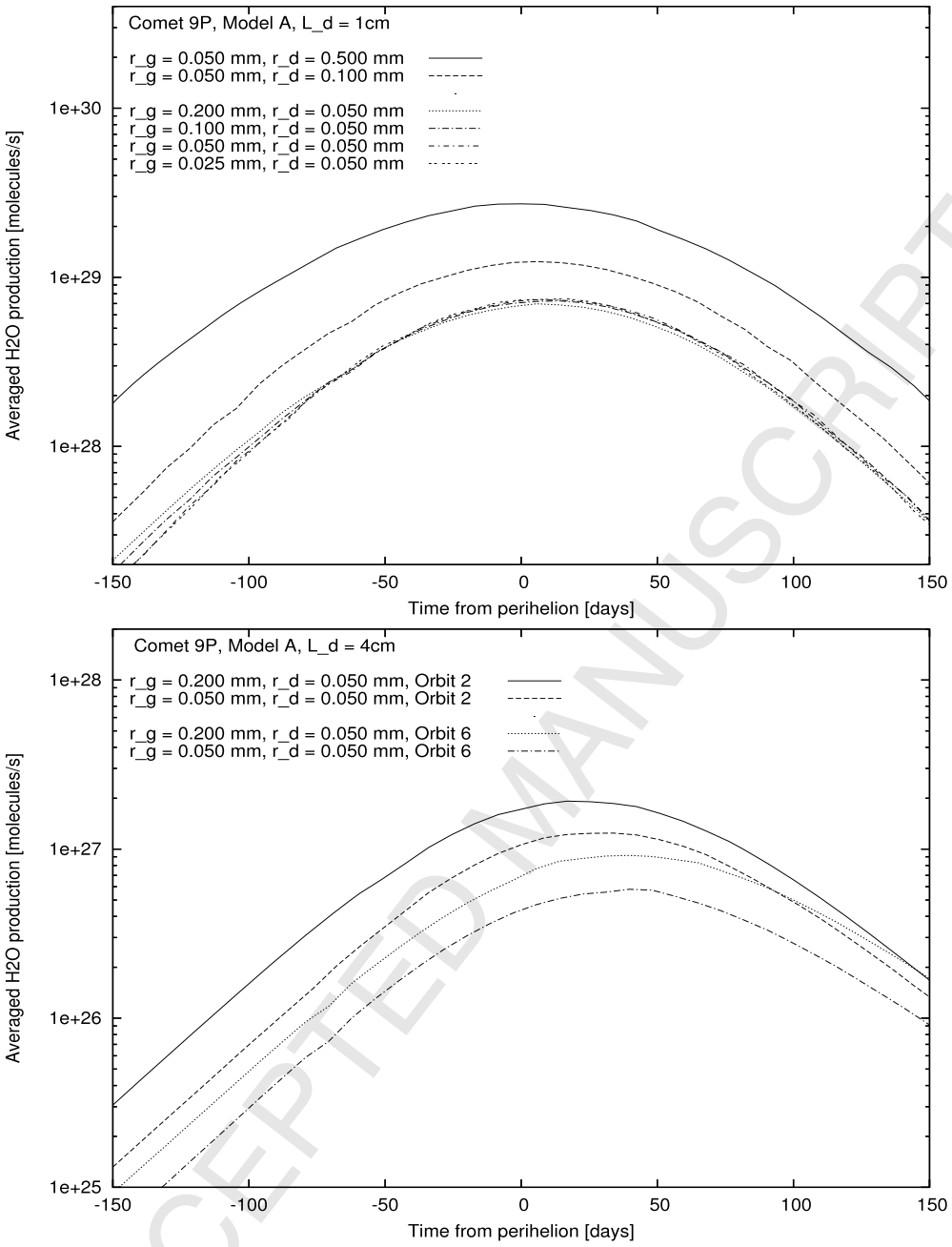

Fig. 4. Influence of the pore radii r_d in the dust mantle, and the grain radii $r_p = r_g$ beneath the dust on the water production curve. Thickness of the dust mantle is constant versus time (Model A), and is uniform: 1 cm (upper panel), and 4 cm (lower panel). The dust thermal conductivity $\lambda_d = 20\,\mathrm{mW\,m^{-1}\,K^{-1}}$, and the porosity of dust mantle $v_d = 0.73$. In the upper panel the curves are drawn for the second orbit.

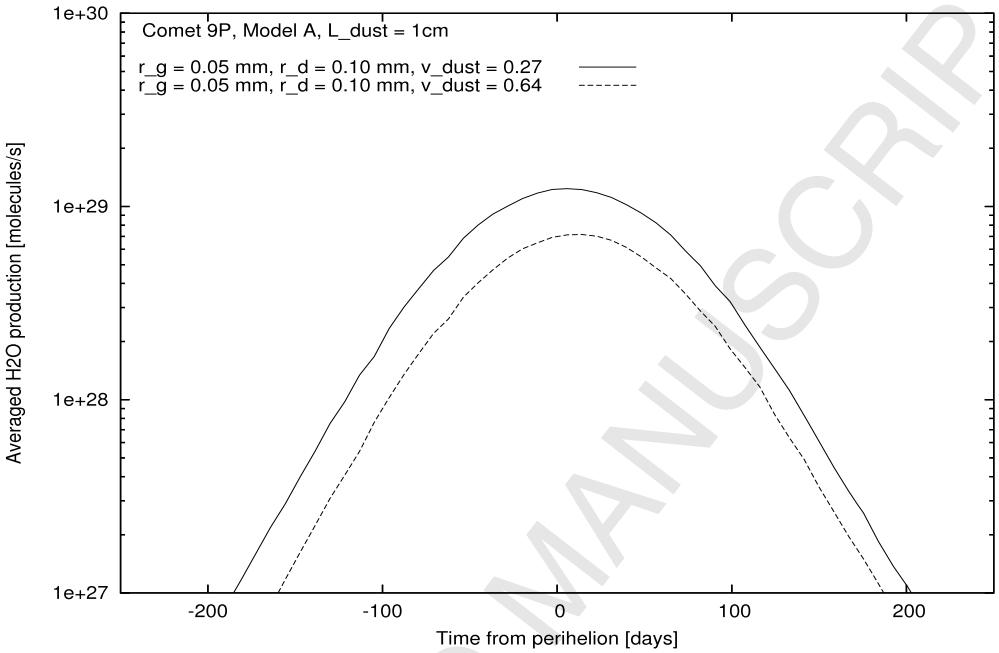

Fig. 5. Influence of density (porosity) of the dust mantle on the water production curve. Thickness of the dust mantle is equal to 1 cm and is constant versus time (Model A), the radii of pores are: $r_d = 0.10$ mm, and $r_p = r_g = 0.05$ mm. The dimensionless density of the dust mantle v_d is either 0.27, or 0.64. These values correspond to the porosity ψ_d equal to 0.73, and 0.26. The dust thermal conductivity $\lambda_d = 20\,\mathrm{mW\,m^{-1}\,K^{-1}}$.

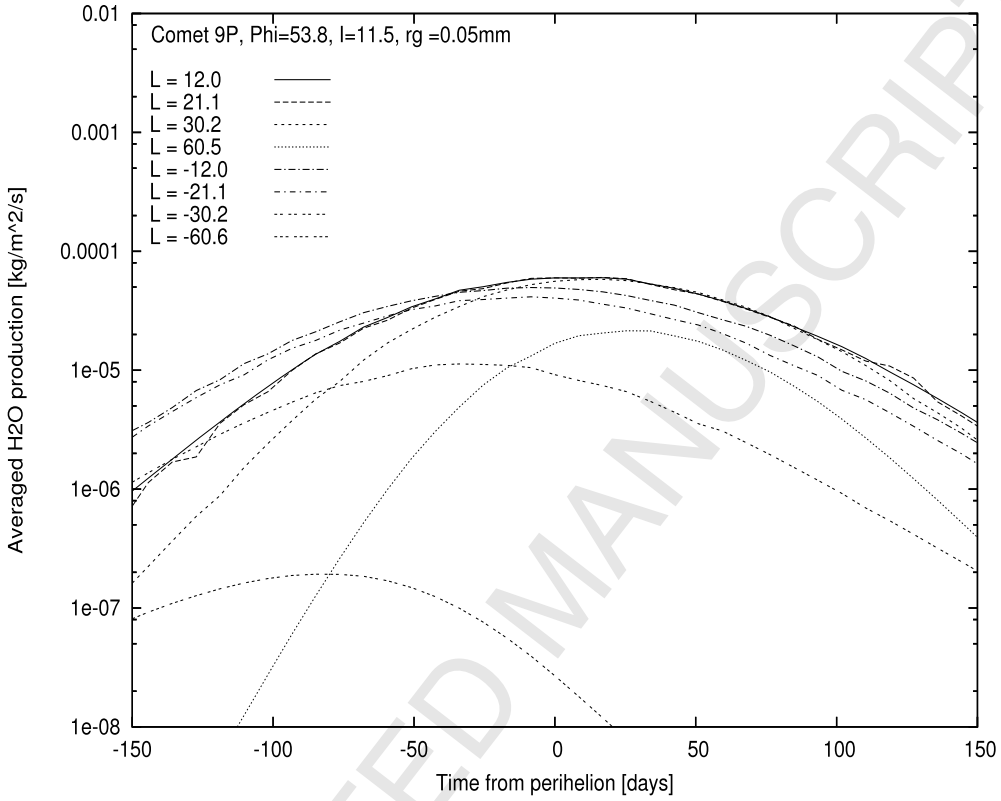

Fig. 6. Theoretical water production versus time at different latitudes. The nucleus is composed of the grains with the radii $r_g = 0.05$mm. Dust layer has thermal conductivity $\lambda_d = 20\ \mathrm{mW\,m^{-1}\,K^{-1}}$. Thickness of the dust mantle is constant versus time and is equal to 1 cm.

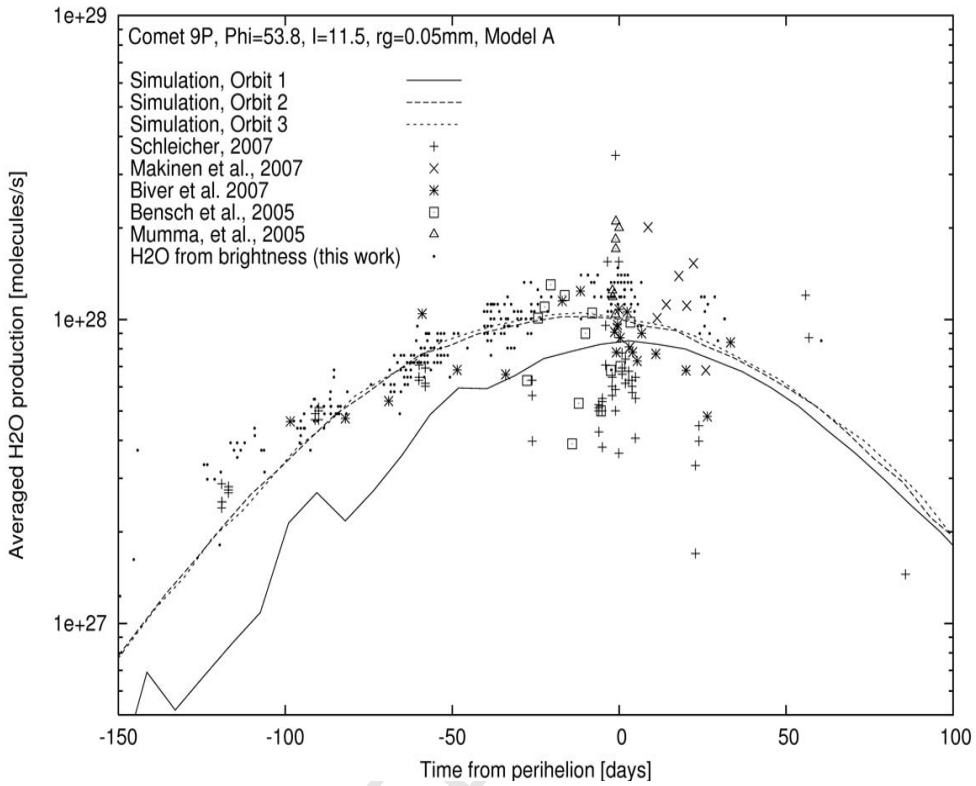

Fig. 7. Theoretical water production curve versus time from perihelion. Thickness of the dust mantle is nonuniform, but constant versus time (Model A). Ice sublimes effectively only from two sectors of the nucleus surface, centered at the latitude -21^o. This sectors are covered by 1 cm thick dust layer, while on the remaining surface dust is thick and prohibits significant sublimation of ice. The dust layer has thermal conductivity $\lambda_d = 20$ mW m^{-1} K^{-1}.

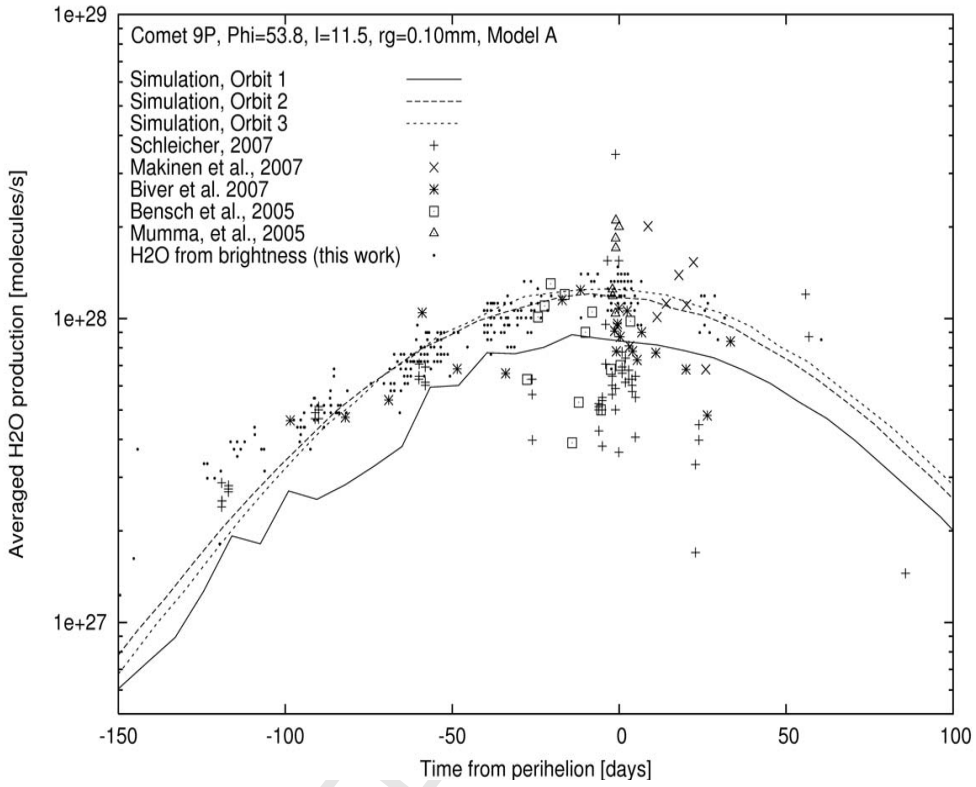

Fig. 8. The same as in Fig. 7, but for the nucleus composed of larger grains r_g = 0.10mm, with larger active area covered by thicker dust. The active areas are now covered by 2cm thick dust mantle and occupy five times larger area. Two sectors are centered at the latitude -12.0^o, four sectors at -21^o and four at -30.2^o.

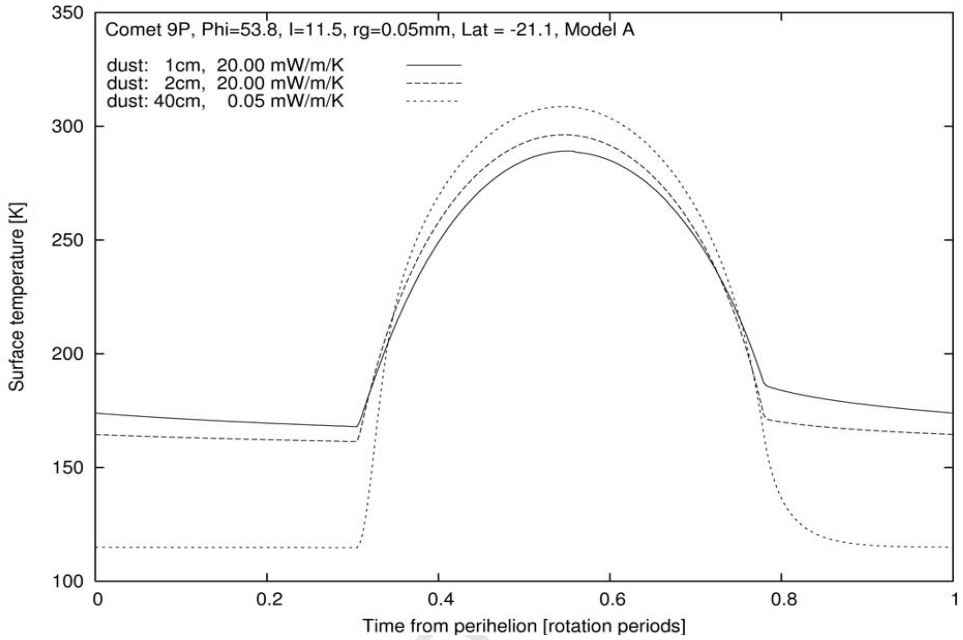

Fig. 9. Diurnal changes of the surface temperature in the selected location at the latitude -21^o, when: (i) $\Delta_d = 1$ cm, $\lambda_d = 20$ mW m^{-1} K^{-1}, and (ii) $\Delta_d = 40$ cm, $\lambda_d = 0.05$ mW m^{-1} K^{-1}. The pore radii are: $r_d = 0.10$mm, $r_p = 0.05$mm.

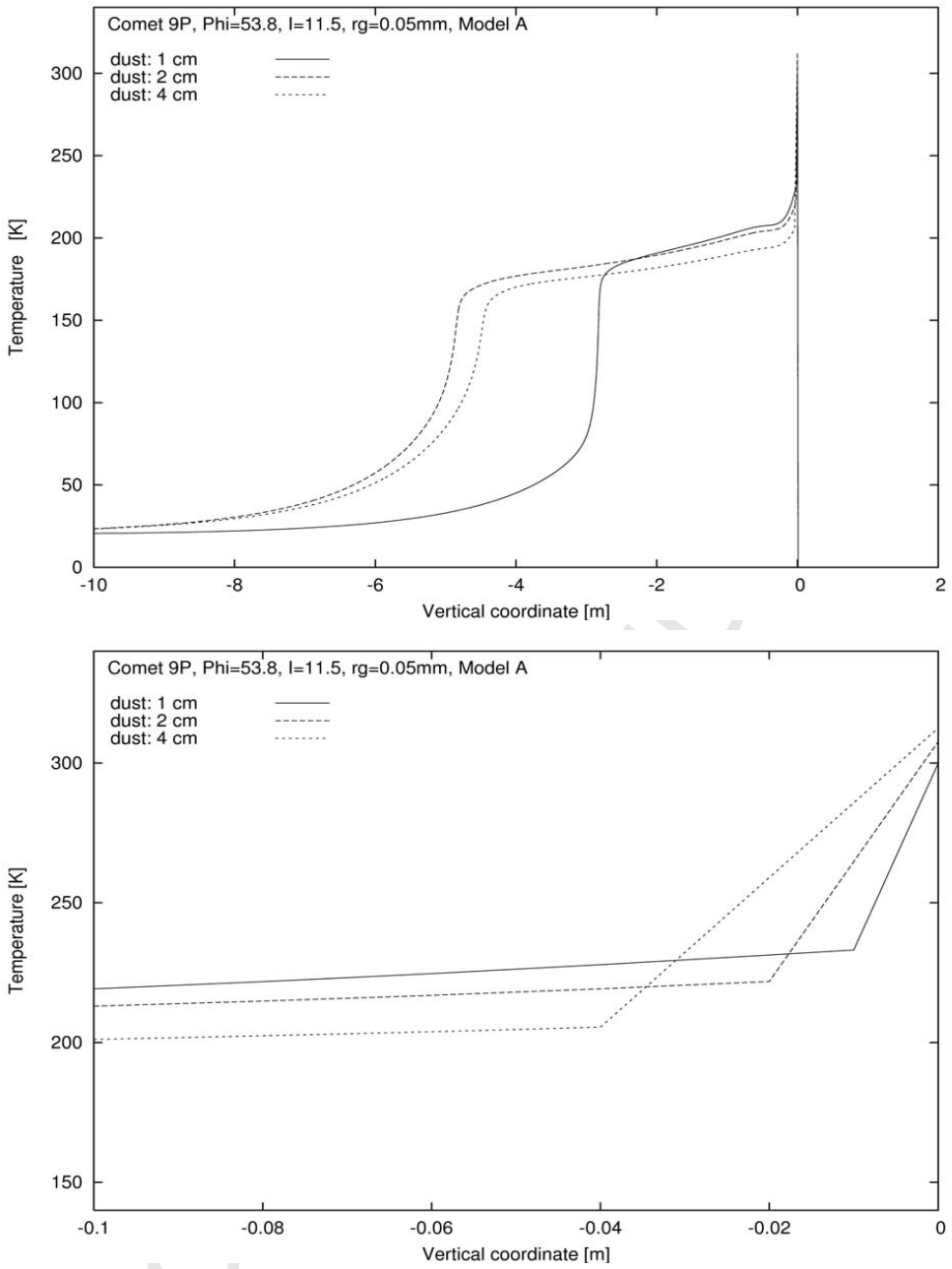

Fig. 10. The subsolar temperature versus depth. The profiles correspond to different thicknesses of the dust layer: 1 cm, 2 cm, and 4 cm. The dust has thermal conductivity $\lambda_d = 20$ mW m^{-1} K^{-1} and the pore radii $r_d = 0.10$mm. In the underlying medium $r_g = 0.05$mm. In the upper panel are shown temperature down to 10 meters below the surface, while the lower panel is only for the topmost 10 centimeters.

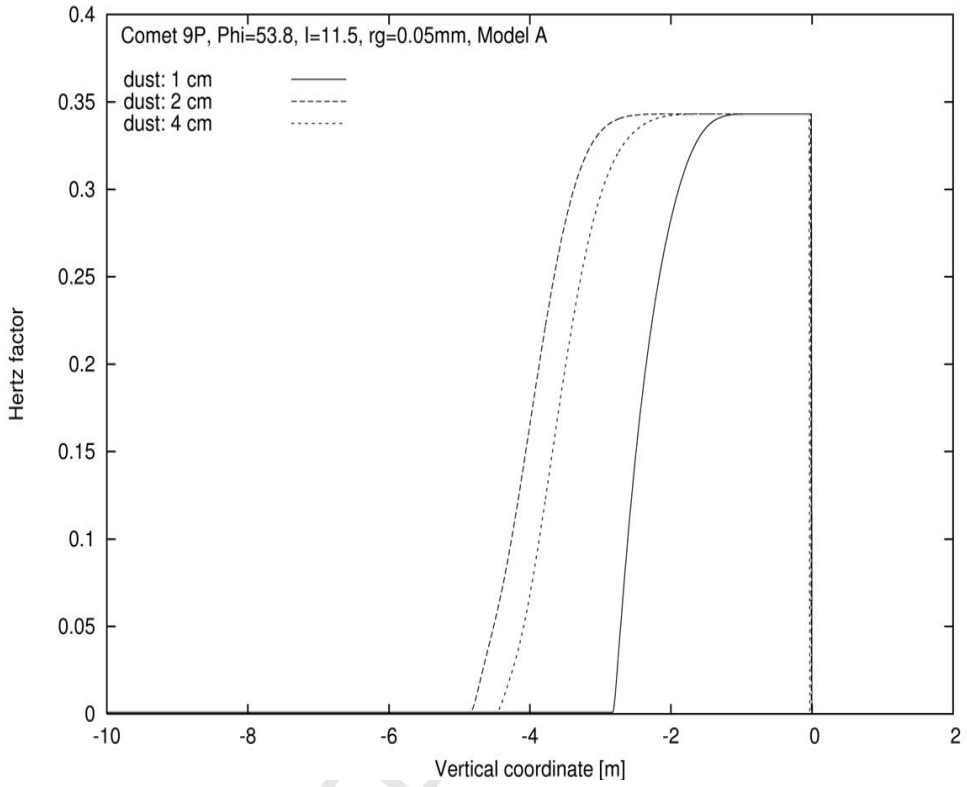

Fig. 11. Hertz factor versus depth. The nucleus is composed of the grains with the radii $r_g = 0.05$mm. Dust layer has thermal conductivity $\lambda_d = 20$ mW m^{-1} K^{-1}. Thickness of the dust mantle is: 1 cm, 2 cm, and 4 cm. The profiles are drawn for the third perihelion passage covered by our simulations.

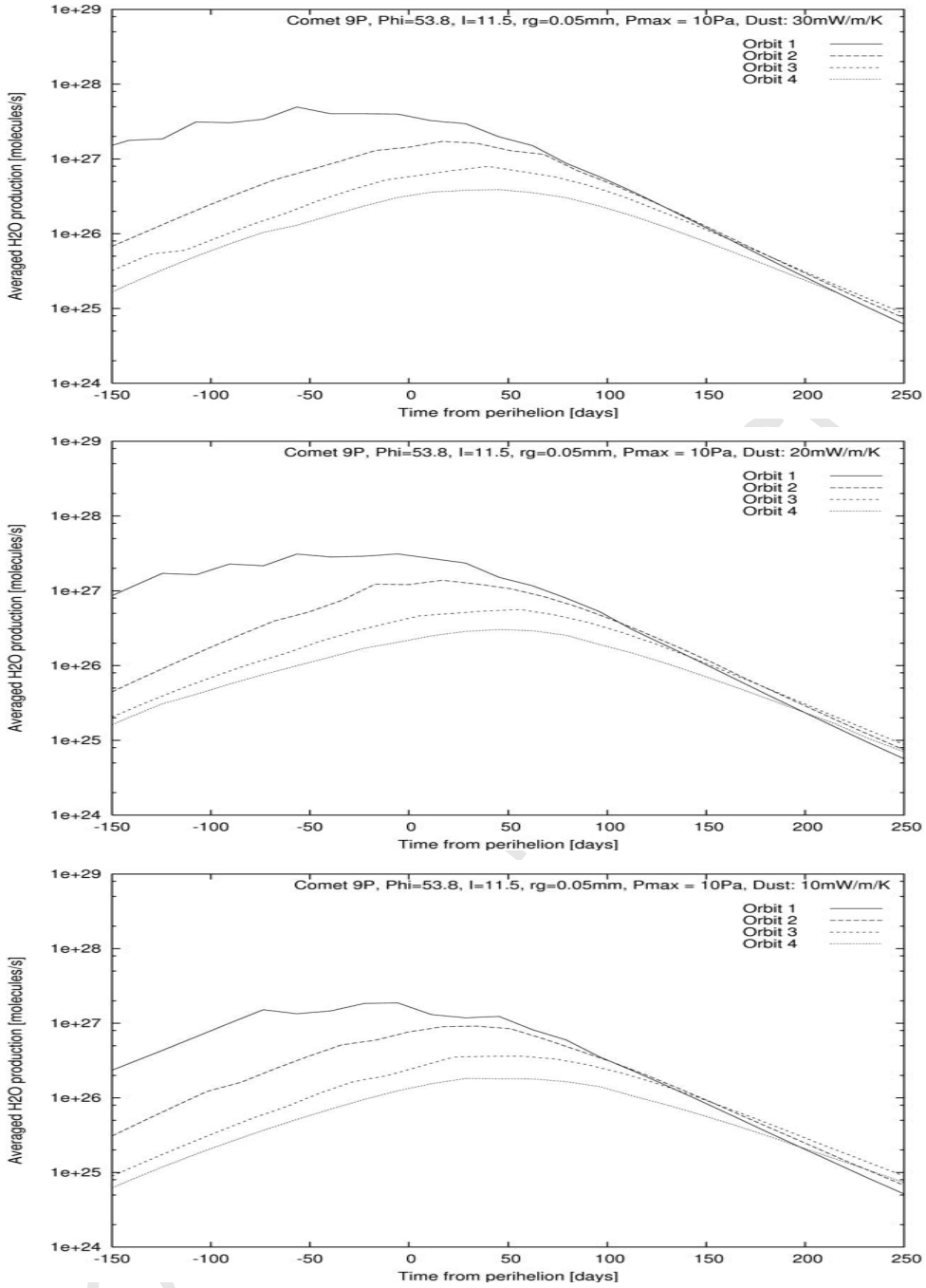

Fig. 12. Theoretical water production curve versus time from perihelion. Thickness of the dust mantle is nonuniform and evolves (Model B). The nucleus is composed of the moderately fine material with $r_g = 0.05$mm. Thermal conductivity of the dust mantle is $\lambda_d = 30\ \mathrm{mW\,m^{-1}\,K^{-1}}$ (upper panel), $\lambda_d = 20\ \mathrm{mW\,m^{-1}\,K^{-1}}$ (middle panel), and $\lambda_d = 10\ \mathrm{mW\,m^{-1}\,K^{-1}}$ (lower panel). The threshold pressure p_{max} is 10 Pa.

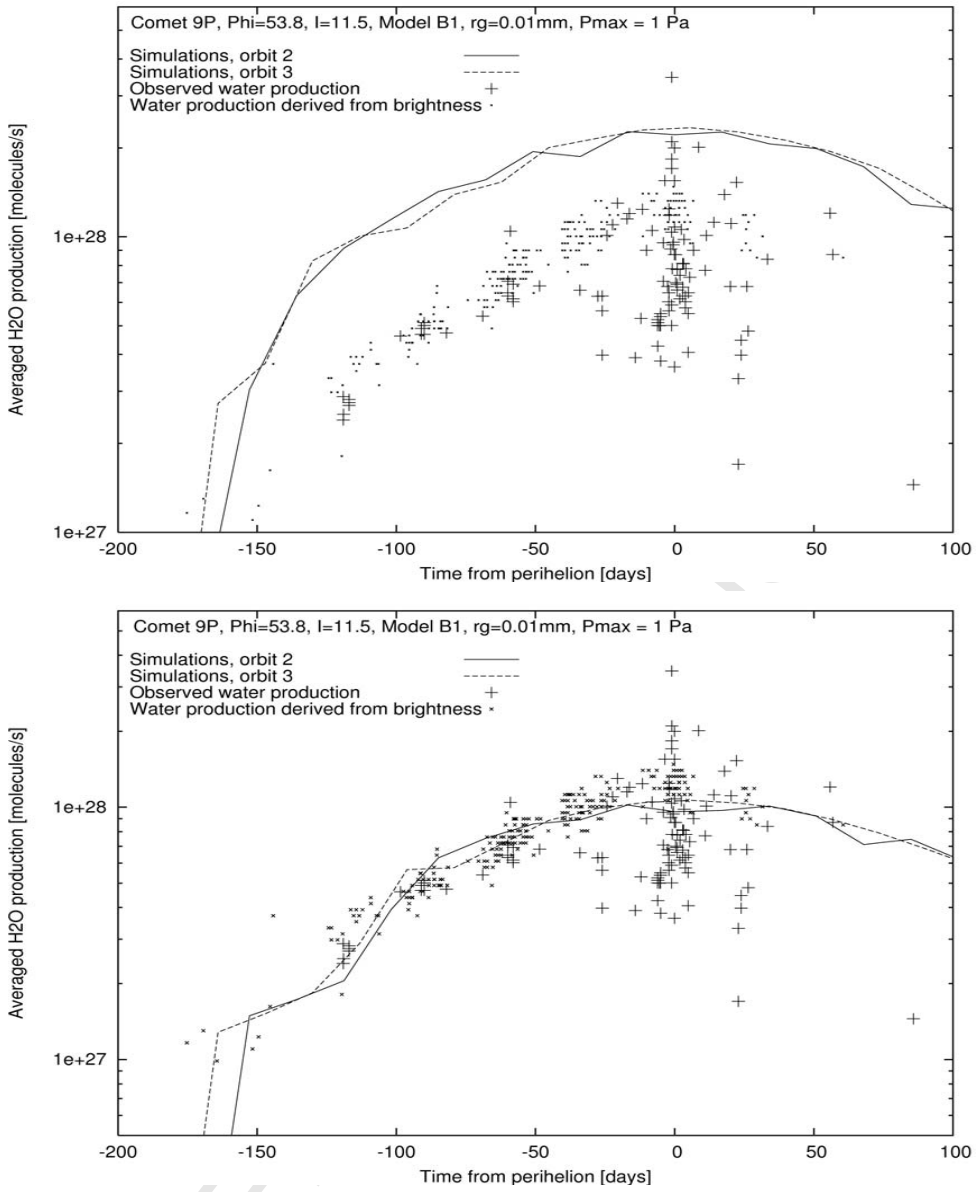

Fig. 13. Theoretical water production curve versus time from perihelion. Thickness of the dust mantle is nonuniform and evolves (Model B). The grain size is $r_g = 0.01$mm, the thermal conductivity $\lambda_d = 30$ mW m^{-1} K^{-1} and the threshold pressure p_{max} is 1 Pa. The initial thickness of dust is: everywhere 1.5cm (upper panel), or very thick except 3 sectors where the dust is 1.5 cm (lower panel). In the latter case the active sectors are located at the latitudes: -21^o (1 sector), and 30^o (2 sectors).